A FINITE-DIFFERENCE, FREQUENCY-DOMAIN NUMERICAL SCHEME FOR THE SOLUTION OF THE LINEARIZED UNSTEADY EULER EQUATIONS

James R. Scott
NASA Lewis Research Center
Cleveland, Ohio 44135

Hafiz M. Atassi
University of Notre Dame
Notre Dame, Indiana 46556

ABSTRACT

A numerical method is developed for solving periodic, three-dimensional, vortical flows around lifting airfoils in subsonic flow. The first-order method that is presented fully accounts for the distortion effects of the nonuniform mean flow on the convected upstream vortical disturbances. The unsteady velocity is split into a vortical component which is a known function of the upstream flow conditions and the Lagrangian coordinates of the mean flow, and an irrotational field whose potential satisfies a nonconstant-coefficient, inhomogeneous, convective wave equation. Using an elliptic coordinate transformation, the unsteady boundary value problem is solved in the frequency domain on grids which are determined as a function of the Mach number and reduced frequency. Extensive comparisons are made with known solutions to unsteady vortical flow problems, and it is seen that the agreement is in general very good for reduced frequencies ranging from 0 up to 4.

I. INTRODUCTION

Most flows encountered in aerodynamics are high speed flows where the Reynolds number is large and the effects of viscosity are confined to small regions such as boundary layers and wakes. Because major portions of these flow fields are essentially inviscid and irrotational, potential flow theory has been used extensively by aerodynamicists in the analysis of flows about streamlined bodies. Today steady potential flow solvers are widely used in the design of aircraft wings, turbomachinery blades, and helicopter rotors.

In many real flow applications, however, the flow is not steady but unsteady. Frequently the unsteadiness in the flow is due to the occurrence of upstream vortical disturbances that are convected downstream and induce an unsteady flow field as they interact with the body. For an aircraft wing, such upstream flow distortion can be caused by atmospheric turbulence. For propeller and turbomachinery blades, the vortical disturbances may be caused by the viscous wakes of an upstream rotor or stator, installation effects, or upstream turbulence.

When viewed from the blade frame of reference, the upstream vortical disturbances will appear as propagating vorticity waves that are called gusts. There are a number of undesirable effects that can be associated with such vortical gusts. They will, for example, induce unsteady forces on the airfoil surface which can cause forced vibrations and radiate noise into the far field. In some instances, the impinging gusts may cause flow separation and loss of aerodynamic performance. For rotating blades, the fundamental frequency of the upstream disturbances will equal the blade passing frequency. If the frequency of the aerodynamic excitation equals a natural frequency of the rotating blades and the amplitude is sufficient, then catastrophic structural failure may result.

Another possible source of unsteadiness in the flow is the unsteady motion of the airfoils or blades themselves. Such unsteady structural motion can be caused by structure-borne vibrations as well as the flow-induced oscillations described above. There can also be unsteady interactions between the airfoil motion and the incident disturbances which can dampen or increase the magnitude of the airfoil unsteady motion.

Because of the undesirable effects associated with these unsteady flows, there is considerable interest in controlling and understanding the aerodynamic excitations which can cause such unsteady blade motion.

Up until recently, most numerical efforts to solve these kinds of unsteady flows concentrated on potential methods. The early work dealt with solving the unsteady small disturbance potential equation as a way of obtaining the unsteady flow around oscillating airfoils or cascades. Later work was directed toward solving the linearized unsteady potential equation and the unsteady full potential equation. Potential methods have proven to work well for oscillating airfoil problems, but unfortunately they cannot adequately account for the vortical part of the flow. Previous potential formulations which have included the effects of the upstream vorticity have invoked the linear thin airfoil approximation and assumed that the imposed vortical gust is convected without distortion by the

nonuniform mean flow. This was the approach used by McCroskey and Goorjian [1] and McCroskey [2]. However, as shown by Goldstein and Atassi [3], Atassi [4], and Scott and Atassi [5], the assumption that the gust is convected without distortion is not justified and is a poor approximation for flows with a spatially varying mean flow. This is especially true for turbomachinery and propeller flow fields where the blades are heavily loaded and there are strong mean flow gradients.

In the past few years, computational efforts in unsteady aerodynamics have concentrated on the so-called primitive variable methods in which the unsteady Euler or Navier-Stokes equations are solved in time along with certain specified boundary conditions. Unlike the potential methods, the primitive variable methods are equally well-suited to both oscillating airfoil problems and flows with convected upstream vorticity. The main difficulty associated with these methods is that they are too expensive to be used for routine engineering calculations such as are encountered in design work. In addition, uncertainties about physically correct far field boundary conditions leaves some question as to the accuracy of the solutions.

In a previous paper [5], the authors presented a linearized unsteady aerodynamic analysis for subsonic vortical flows around lifting airfoils which represents an alternative to the potential and primitive variable methods. The analysis that was presented in [5] offers the computational efficiency of potential methods, but at the same time accounts for the convection and distortion of the upstream vorticity by the nonuniform mean flow. Our analysis is therefore equally well-suited to vortical flow problems as well as to oscillating airfoil problems. In addition, since our linearization is about the nonuniform mean flow, the full nonlinear effects of the mean flow are accounted for. Only the unsteady part of the flow is linearized. These features, coupled with the inherent efficiency of the linearized approach, make our analysis an ideal solution method for unsteady aerodynamic flow fields.

In [5] we presented the mathematical formulation of the general linearized boundary value problem, and demonstrated the capabilities of our approach by presenting numerical solutions for a large variety of unsteady vortical flows. The numerical results presented showed in detail the effects of airfoil thickness, angle of attack, camber, and Mach number on the unsteady lift and moment of isolated airfoils subjected to periodic vortical gusts in subsonic flows.

In the present paper our major purpose is to present the details of the frequency domain numerical scheme that has been developed to implement our linearized unsteady aerodynamic analysis. Since we presented the full formulation of the analysis in [5], we will only summarize the resulting boundary value problem in the present paper. This will be done in the following section. Following that will be the main section of the paper which presents our frequency domain numerical scheme. Finally, in Section IV, we present a large variety of numerical results which demonstrate the validation of our codes.

II. LINEARIZED UNSTEADY AERODYNAMIC FORMULATION

Consider an inviscid, compressible flow past a two-dimensional airfoil placed at nonzero incidence to a stream with uniform upstream velocity U_∞ in the x_1 direction. We assume in the present discussion that the fluid is an ideal, non-heat conducting gas with constant specific heats, and that there are no shocks in the flow. Under the above assumptions there will be a steady potential flow around the airfoil so that we may write

$$\vec{U}_0(\vec{x}) = \vec{\nabla}\Phi_0, \tag{2.1}$$

where 0 subscripts are used to denote steady mean flow quantities.

Let us assume that far upstream an unsteady vortical disturbance is imposed on the flow. The only restriction that we place on the upstream disturbance is that it can be expressed as a generalized Fourier integral so that we may write

$$\vec{u}_\infty(\vec{x} - \vec{i}U_\infty t) = \int_{\vec{k}} \vec{a}(\vec{k}) e^{i\vec{k}\cdot(\vec{x}-\vec{i}U_\infty t)} d\vec{k} \tag{2.2}$$

and in addition, that its length scale l' and characteristic velocity u_∞ are such that the condition

$$\frac{c}{U_\infty} \ll \frac{l'}{u_\infty} \tag{2.3}$$

is satisfied, where c is the airfoil chord length. We thus require that the time scale associated with the mean flow be an order of magnitude less than the time scale associated with the upstream unsteady disturbances. Since our concern is with flows that have large scale upstream disturbances in which l' is the same order of magnitude as the chord length c, condition (2.3) essentially reduces to the requirement that $u_\infty \ll U_\infty$.

Since we present a linearized mathematical formulation, we may without loss of generality consider a single Fourier component of the incident vortical disturbance, and solve for more general disturbances by superposition. We therefore consider incident vortical gusts of the form

$$\vec{u}_\infty = \vec{a} e^{i\vec{k}\cdot(\vec{X}-\vec{i}U_\infty t)}, \tag{2.4}$$

where $\vec{a}$ and $\vec{k}$ must satisfy

$$\vec{a}\cdot\vec{k} = 0 \tag{2.5}$$

to ensure that the continuity equation is satisfied.

In general, the components of $\vec{X}$ in equation (2.4) are not the spatial coordinates, but rather are Lagrangian coordinates of the mean flow. For the case of two-dimensional mean flow the components of $\vec{X}$ are given by

$$X_2 = \frac{\Psi_0}{\rho_\infty U_\infty} \tag{2.6}$$

and

$$X_3 = x_3, \tag{2.7}$$

where Ψ_0 is the stream function of the mean flow and x_3 is the spatial coordinate in the spanwise direction. The component X_1 is defined by

$$X_1 = U_\infty \Delta, \tag{2.8}$$

where Δ is the Lighthill "drift" function [6], which can be expressed in terms of Φ_0 and Ψ_0 as

$$\Delta = \frac{\Phi_0}{{U_\infty}^2} + \int_{-\infty}^{\Phi_0} (\frac{1}{{U_0}^2} - \frac{1}{{U_\infty}^2}) d\Phi_0, \tag{2.9}$$

where the integration is carried out on $\Psi_0 =$ constant. The difference in Δ between two points on a streamline is the time it takes a mean flow fluid particle to traverse the distance between those two points. Note that for the thin airfoil case in which the mean flow is a uniform parallel flow, the components of $\vec{X}$ reduce precisely to the spatial coordinates.

We assume that the total unsteady flow field can be represented by

$$\vec{U}(\vec{x},t) = \vec{U}_0(\vec{x}) + \vec{u}(\vec{x},t) \tag{2.10}$$

$$p(\vec{x},t) = p_0(\vec{x}) + p'(\vec{x},t) \tag{2.11}$$

$$\rho(\vec{x},t) = \rho_0(\vec{x}) + \rho'(\vec{x},t) \tag{2.12}$$

$$s(\vec{x},t) = s_0 + s'(\vec{x},t) \tag{2.13}$$

where the entropy s_0 is constant, and $\vec{u}$, p', ρ', and s' are the unsteady perturbation velocity, pressure, density and entropy, respectively. Quantities with 0 subscripts are the steady mean flow quantities which are assumed to be known. Note that these quantities obey the steady nonlinear equations of motion, so that the linearization of the unsteady flow is about the fully nonlinear mean flow.

Substituting relations (2.10) - (2.13) into the nonlinear Euler equations and neglecting products of small quantities, one obtains the linearized continuity, momentum, and energy equations

$$\frac{D_0\rho'}{Dt} + \rho'\vec{\nabla}\cdot\vec{U}_0 + \vec{\nabla}\cdot(\rho_0\vec{u}) = 0 \tag{2.14}$$

$$\rho_0(\frac{D_0\vec{u}}{Dt} + \vec{u}\cdot\vec{\nabla}\vec{U}_0) + \rho'\vec{U}_0\cdot\vec{\nabla}\vec{U}_0 = -\vec{\nabla}p' \tag{2.15}$$

$$\frac{D_0 s'}{Dt} = 0, \tag{2.16}$$

where $\frac{D_0}{Dt} = \frac{\partial}{\partial t} + \vec{U}_0\cdot\vec{\nabla}$ is the convective derivative associated with the mean flow.

It is shown in References 7 and 8 that if the unsteady velocity is decomposed into the sum of a known vortical component and an unknown potential component, then the

problem for determining the unsteady flow may be reduced to solving a single, non-constant coefficient, inhomogeneous convective wave equation which may be written

$$\frac{D_0}{Dt}\left(\frac{1}{{c_0}^2}\frac{D_0\phi}{Dt}\right) - \frac{1}{\rho_0}\vec{\nabla}\cdot(\rho_0\vec{\nabla}\phi) = \frac{1}{\rho_0}\vec{\nabla}\cdot(\rho_0\vec{u}^{(R)}), \tag{2.17}$$

where

$$\vec{u}(\vec{x},t) = \vec{u}^{(R)} + \vec{\nabla}\phi. \tag{2.18}$$

The unsteady pressure is related to ϕ through the equation

$$p' = -\rho_0(\vec{x})\frac{D_0\phi}{Dt}. \tag{2.19}$$

The vortical velocity $\vec{u}^{(R)}$ is a known function of the mean flow Lagrangian coordinates and the upstream vortical disturbances and is given by

$$\vec{u}^{(R)} = [\vec{\nabla}(\vec{a}\cdot\vec{X})]e^{i\vec{k}\cdot(\vec{X}-\vec{i}U_\infty t)} + \vec{\nabla}\tilde{\phi}, \tag{2.20}$$

where

$$\tilde{\phi} = \frac{i}{k_1}\left(a_1 + \frac{a_2k_1 - a_1k_2}{1 + ia_0U_\infty k_1}\frac{1-e^{-ik_2X_2}}{k_2}\right)e^{i\vec{k}\cdot(\vec{X}-\vec{i}U_\infty t)}, \tag{2.21}$$

and

$$\vec{a} = (a_1, a_2, a_3) \qquad \text{and} \quad a_0 = -\left(\frac{\partial U_0}{\partial n}\right)_S^{-1}. \tag{2.22}$$

Here n denotes the direction of the outward unit normal, S denotes the stagnation point near the airfoil leading edge, and $U_0 = |\vec{U_0}|$ is the magnitude of the mean velocity. (See [5] or [8] for more details concerning the purpose and derivation of the function $\tilde{\phi}$.)

Finally, the potential ϕ must satisfy the boundary conditions

$$\vec{\nabla}\phi\cdot\vec{n} = 0 \qquad \text{airfoil surface} \tag{2.23}$$

$$\frac{D_0}{Dt}(\triangle\phi) = 0 \qquad \text{wake} \tag{2.24a}$$

$$\triangle[\vec{\nabla}\phi\cdot\vec{n}] = 0 \qquad \text{wake} \tag{2.24b}$$

$$\vec{\nabla}\phi \to -\vec{\nabla}\tilde{\phi} \quad \text{as} \quad x_1 \to -\infty, \tag{2.25}$$

where equation (2.23) is the impermeability condition at the airfoil surface, equations (2.24a) and (2.24b) impose continuity of the pressure and normal velocity across the wake, and equation (2.25) ensures that $\vec{u}(\vec{x},t) \to \vec{u}_\infty(\vec{x},t)$ as $x_1 \to -\infty$.

The linearized boundary value problem for the unsteady gust response problem thus consists of the governing equation (2.17) and boundary conditions (2.23) – (2.25), together with the requirement that ϕ is continous at the airfoil trailing edge.

III. NUMERICAL SCHEME

Reformulation and Nondimensionalization of the Boundary Value Problem

For numerical purposes it is necessary to reformulate the boundary value problem presented in the previous section into a form more suitable for numerical computations. Of particular concern is condition (2.25). In order to facilitate the implementation of the far field boundary condition, it is convenient to replace ϕ by a function whose gradient vanishes as $r \to \infty$, where r is the distance from the airfoil center.

To this end, we introduce the potential functions ϕ_1 and ϕ_2, where

$$\phi = \phi_1 - \phi_2 \tag{3.1}$$

and ϕ_2 is a known function which is constructed such that

$$|\phi_2 - \tilde{\phi}| \to 0 \qquad \text{as} \quad r \to \infty. \tag{3.2}$$

Equation (3.1) together with conditions (2.25) and (3.2) then show that the new potential function ϕ_1 will satisfy

$$\vec{\nabla}\phi_1 \to \vec{\nabla}\phi_2 - \vec{\nabla}\tilde{\phi} \to 0 \qquad \text{as} \quad r \to \infty. \tag{3.3}$$

The problem may then be reformulated in terms of the unknown potential ϕ_1.

To satisfy condition (3.2), the function ϕ_2 must take the form

$$\phi_2 = \frac{i}{k_1}\left(a_1 + \frac{a_2 k_1 - a_1 k_2}{1 + i a_0 U_\infty k_1}\frac{1 - e^{-ik_2 X_2}}{k_2}\right)e^{i\vec{k}\cdot(\vec{X}_e - \vec{i}U_\infty t)}, \tag{3.4}$$

where the vector $\vec{X}_e$ satisfies

$$|\vec{X}_e - \vec{X}| \to 0 \qquad \text{as} \quad r \to \infty. \tag{3.5}$$

To satisfy this condition for the general problem of vortical flows around lifting airfoils, we define $\vec{X}_e$ as follows:

$$X_{e,1} = \frac{\Phi_0}{U_\infty} - \frac{\Gamma}{\pi U_\infty}\mathrm{sgn}(\Psi_0)\left[\frac{\pi}{2} + \mathrm{sgn}(\Psi_0)\tan^{-1}\left(\frac{\rho_\infty \Phi_0}{\beta_\infty \Psi_0}\right)\right]\left[1 - e^{-(\Phi_0^2 + \frac{\Psi_0^2}{\rho_\infty^2})(\frac{2}{cU_\infty})^2}\right] \tag{3.6}$$

$$X_{e,2} = X_2 \tag{3.7}$$

$$X_{e,3} = X_3. \tag{3.8}$$

The expression for $X_{e,1}$ is obtained by making a far field expansion of Lighthill's drift function Δ in terms of Φ_0 and Ψ_0. Note that the first term in the expansion is just $\frac{\Phi_0}{U_\infty}$, and that the second term arises due to the circulation around the airfoil. Since the second

term vanishes for airfoils with zero circulation, it is clear that the formulation of the source term for nonlifting airfoils is much simpler than for lifting airfoils.

We also point out that the first factor in brackets in equation (3.6) is discontinuous and undefined at the points on the airfoil where $\Phi_0 = 0, \Psi_0 = 0^+$ and $\Phi_0 = 0, \Psi_0 = 0^-$. The second factor in brackets is not part of the expansion itself, but is included to remove the discontinuity in $X_{e,1}$. By including the second factor in brackets and defining $X_{e,1} = 0$ at $\Phi_0 = 0$, $\Psi_0 = 0$, we obtain an expression for $X_{e,1}$ which is everywhere continuous. It is important that $X_{e,1}$ be continuous along the airfoil surface, for if it were not, the potential function ϕ_1 would have to satisfy a discontinuous airfoil boundary condition. (See condition (3.10) below.) By defining $X_{e,1}$ as in (3.6), we obtain an expression for $\vec{X}_e$ which is everywhere continuous and also ensures that conditions (3.5) and (3.2) will be satisfied for both lifting and nonlifting airfoils.

Finally, the parameter $\beta_\infty = \sqrt{1 - {M_\infty}^2}$, where M_∞ is the free stream Mach number, and c is the airfoil chord length. The β_∞ term arises due to a Gothert's rule correction on the mean velocity so that the expression for $X_{e,1}$ is valid for both compressible and incompressible flows.

Before presenting the reformulated boundary value problem in terms of the potential ϕ_1, we present the nondimensionalization of the problem. We normalize as follows:

$x_1, x_2, x_3, X_1, X_2, X_3, X_{e,1}$	by	$\frac{c}{2}$
Φ_0, Γ	by	$\frac{c}{2}U_\infty$
Ψ_0	by	$\frac{c}{2}\rho_\infty U_\infty$
U_0, c_0	by	U_∞
ρ_0	by	ρ_∞
p'	by	$\rho_\infty U_\infty \lvert\vec{a}\rvert$
t, Δ	by	$\frac{c}{2U_\infty}$
ω	by	$\frac{2U_\infty}{c}$
k_1, k_2, k_3	by	$\frac{2}{c}$
$\phi, \tilde{\phi}, \phi_1, \phi_2$	by	$\frac{c}{2}\lvert\vec{a}\rvert$
$\vec{a}$	by	$\lvert\vec{a}\rvert$

The normalized wave number $k_1 = \frac{\omega c}{2U_\infty}$, where ω and U_∞ are the dimensional angular frequency and free stream velocity, respectively, is called the reduced frequency.

We will assume throughout the remainder of the present section, unless stated otherwise, that all quantities are nondimensional.

The governing equation for ϕ_1 is then

$$\frac{D_0}{Dt}\left(\frac{1}{{c_0}^2}\frac{D_0\phi_1}{Dt}\right) - \frac{1}{\rho_0}\vec{\nabla}\cdot(\rho_0\vec{\nabla}\phi_1) = \frac{1}{\rho_0}\vec{\nabla}\cdot(\rho_0\vec{u}^{(R)})$$

$$+ \frac{D_0}{Dt}\left(\frac{1}{{c_0}^2}\frac{D_0\phi_2}{Dt}\right) - \frac{1}{\rho_0}\vec{\nabla}\cdot(\rho_0\vec{\nabla}\phi_2) \tag{3.9}$$

and the boundary conditions are

$$\vec{\nabla}\phi_1 \cdot \vec{n} = \vec{\nabla}\phi_2 \cdot \vec{n} \qquad \text{airfoil surface} \tag{3.10}$$

$$\frac{D_0}{Dt}[\Delta(\phi_1 - \phi_2)] = 0 \qquad \text{wake} \tag{3.11a}$$

$$\Delta[\vec{\nabla}(\phi_1 - \phi_2) \cdot \vec{n}] = 0 \qquad \text{wake} \tag{3.11b}$$

$$\vec{\nabla}\phi_1 \to 0 \quad \text{as} \quad x_1 \to -\infty. \tag{3.12}$$

For completeness we also present the nondimensional expressions for the potential functions $\tilde{\phi}$ and ϕ_2, for the unsteady velocity and pressure, and for the upstream velocity disturbances.

$$\tilde{\phi} = \frac{i}{k_1}(a_1 + \frac{a_2 k_1 - a_1 k_2}{1 + i a_0 k_1}\frac{1 - e^{-ik_2 X_2}}{k_2})e^{i\vec{k}\cdot\vec{X} - ik_1 t} \tag{3.13}$$

$$\phi_2 = \frac{i}{k_1}(a_1 + \frac{a_2 k_1 - a_1 k_2}{1 + i a_0 k_1}\frac{1 - e^{-ik_2 X_2}}{k_2})e^{i\vec{k}\cdot\vec{X}_e - ik_1 t}, \tag{3.14}$$

where

$$X_1 = \Delta, \quad X_2 = X_{e,2} = \Psi_0, \quad X_3 = X_{e,3} = x_3 \tag{3.15}$$

$$X_{e,1} = \Phi_0 - \frac{\Gamma}{\pi}\text{sgn}(\Psi_0)[\frac{\pi}{2} + \text{sgn}(\Psi_0)\tan^{-1}(\frac{\Phi_0}{\beta_\infty \Psi_0})][1 - e^{-(\Phi_0^2 + \Psi_0^2)}] \tag{3.16}$$

$$\vec{u}(\vec{x}, t) = \vec{u}^{(R)} + \vec{\nabla}(\phi_1 - \phi_2) \tag{3.17}$$

where

$$\vec{u}^{(R)} = [\vec{\nabla}(\vec{a} \cdot \vec{X})]e^{i\vec{k}\cdot\vec{X} - ik_1 t} + \vec{\nabla}\tilde{\phi}. \tag{3.18}$$

$$p' = -\rho_0(\vec{x})\frac{D_0(\phi_1 - \phi_2)}{Dt}. \tag{3.19}$$

$$\vec{u}_\infty = \vec{a}e^{i\vec{k}\cdot\vec{X} - ik_1 t} \tag{3.20}$$

Determination of Mean Potential Flow

In order to obtain numerical solutions to equation (3.9) and its associated boundary conditions, one must first obtain the steady potential flow about the airfoil for the given flow conditions. This will in general require the use of a standard potential flow solver such as FLO36.[9]

However, an examination of equations (3.13) through (3.18) indicates that the most natural choice of independent variables in which to solve equation (3.9) are Φ_0 and Ψ_0, the mean flow potential and stream functions. Since standard potential flow codes solve

the steady problem in terms of the spatial coordinates x_1 and x_2, there is some difficulty in obtaining the steady solution as a function of Φ_0 and Ψ_0.

Another difficulty arises due to the fact that the grids used by steady flow solvers are not suitable for the unsteady calculation. As reported in References 10 and 11, accurate solution of equation (3.9) over a large range of flow conditions requires using grids which are determined as a function of both the reduced frequency k_1 and the free stream Mach number M_∞. This means that in general it will be necessary to interpolate the solution from the steady grid onto the appropriate unsteady grid.

Because of the loss of accuracy that can result from such an interpolation process, and also because of the need to know the mean flow as a function of Φ_0 and Ψ_0, an analytical scheme that can obtain the compressible, subsonic flow about isolated airfoils was developed. The scheme is based on the idea that, except for a small inner region surrounding the airfoil, the flow gradients are not too large. Thus in the large outer region extending to infinity, the mean flow is essentially governed by a set of linear equations. As a result, one can use Gothert's Rule, whereby the compressible flow about a given airfoil can be obtained from the incompressible flow about a similar airfoil.

If we let α_C, θ_C, and γ_C denote the angle of attack, thickness ratio, and camber ratio of the given airfoil in a compressible flow, then the transformed airfoil for the incompressible flow field has angle of attack, thickness ratio, and camber ratio given by

$$\left.\begin{aligned} \alpha_I &= \beta_\infty \, \alpha_C \\ \theta_I &= \beta_\infty \, \theta_C \\ \gamma_I &= \beta_\infty \, \gamma_C \end{aligned}\right\} \tag{3.21}$$

where I subscripts denote quantities from the incompressible flow field. Using dimensional quantities and denoting the compressible velocity by $(U_\infty + u_C, v_C)$ at the point (x, y) and the incompressible velocity by $(U_\infty + u_I, v_I)$ at the point (x_I, y_I), the spatial coordinates and velocity in the compressible and incompressible planes are related by

$$x = x_I \tag{3.22a}$$

$$y = \frac{y_I}{\beta_\infty} \tag{3.22b}$$

and

$$u_C = \frac{u_I}{{\beta_\infty}^2} \tag{3.23a}$$

$$v_C = \frac{v_I}{\beta_\infty}. \tag{3.23b}$$

It is assumed here that the free stream velocity U_∞ is aligned with the x axis, and that the angle of attack, thickness ratio, and camber ratio of the airfoil are such that the perturbation velocities are small compared to U_∞. The potential and stream functions of

the compressible flow field are then related to the potential and stream functions of the incompressible flow field by

$$\Phi_0 - U_\infty x = \frac{1}{{\beta_\infty}^2}(\Phi_I - U_\infty x_I) \tag{3.24a}$$

$$\Psi_0 - U_\infty y = \frac{1}{\beta_\infty}(\Psi_I - U_\infty y_I) \tag{3.24b}$$

Using (3.22), and assuming that all quantities have been nondimensionalized as in the previous section, equations (3.24) can be rewritten

$$\Phi_I - M_\infty^2 x_I = \beta_\infty^2 \Phi_0 \tag{3.25a}$$

$$\Psi_I = \beta_\infty \Psi_0 \tag{3.25b}$$

The problem is then, given (Φ_0, Ψ_0), solve equations (3.25) for (Φ_I, Ψ_I) and then use relations (3.22) and (3.23) to determine the spatial coordinates (x, y) and velocity components (u_C, v_C) of the compressible flow field. If this can be done, then we have the compressible flow field determined as a function of (Φ_0, Ψ_0). Note that this assumes that we can determine (x_I, y_I) and (u_I, v_I) as functions of (Φ_I, Ψ_I). Since there is a one to one correspondence between (x_I, y_I) and (Φ_I, Ψ_I), and between (u_I, v_I) and (Φ_I, Ψ_I), this is not a difficulty. At the least, it can always be done numerically. For the special case of Joukowski airfoils, however, it is possible to express the complex potential (Φ_I, Ψ_I) in terms of the polar coordinates (r, θ), and then obtain (x_I, y_I) and (u_I, v_I) through known functional expressions of (r, θ).

For the case of incompressible flow around a Joukowski airfoil the complex potential is given by

$$\Phi_I + i\,\Psi_I = \zeta' e^{-i\alpha_I} + \frac{a^2 e^{i\alpha_I}}{\zeta'} + \frac{\Gamma_I}{2\pi i}\ln(\frac{\zeta'}{a}) + K \tag{3.26}$$

where K is an arbitrary constant and

$$\zeta' = \zeta - \zeta_{0'} = re^{i\theta}. \tag{3.27}$$

Here $\zeta_{0'} = -\epsilon + i\epsilon'$ is a complex constant, and the parameters a, ϵ, and ϵ' depend on the airfoil geometry. Γ_I is the steady circulation around the airfoil and is given by

$$\Gamma_I = -4\pi a \sin(\alpha_I + \beta) \tag{3.28}$$

where β is defined by

$$\sin\beta = \frac{\epsilon'}{a}. \tag{3.29}$$

The spatial coordinates (x_I, y_I) are determined from r and θ through the Joukowski transformation

$$x_I + i\, y_I = \zeta + \frac{d^2}{\zeta} \tag{3.30}$$

where the parameter d satisfies

$$(\epsilon + d)^2 + \epsilon'^2 = a^2. \tag{3.31}$$

Finally, the velocity components (u_I, v_I) are given by

$$u_I - i\, v_I = \frac{\zeta^2[\zeta' + ae^{i(2\alpha_I+\beta)}]}{(\zeta + d)\zeta'^2} \quad - \quad 1. \tag{3.32}$$

Using relations (3.26) through (3.30), equations (3.25) can be expressed in terms of r and θ as

$$\left.\begin{aligned} &(r + \tfrac{a^2}{r})\cos(\theta - \alpha_I) - [2a\sin(\alpha_I + \beta)]\theta + K \\ &-M_\infty^2[r\cos\theta - \epsilon + \tfrac{d^2(r\cos\theta-\epsilon)}{(r\cos\theta-\epsilon)^2+(r\sin\theta+\epsilon')^2}] = \beta_\infty^2\Phi_0 \\ &(r - \tfrac{a^2}{r})\sin(\theta - \alpha_I) + 2a\sin(\alpha_I + \beta)\ln(\tfrac{r}{a}) = \beta_\infty\Psi_0 \end{aligned}\right\} \tag{3.33}$$

If for given Φ_0 and Ψ_0 we can solve equations (3.33) for r and θ, then equations (3.30) and (3.32) can be used to get (x_I, y_I) and (u_I, v_I), and equations (3.22) and (3.23) can be used to obtain (x, y) and (u_c, v_c). Once we have obtained (u_c, v_c), the other mean flow quantities can then be obtained from Bernoulli's law for polytropic gases.

We note that, while the system of equations (3.33) is highly nonlinear in the unknowns r and θ, it can be routinely solved by two-dimensional Newton iteration. Once a subroutine has been developed to solve equations (3.33), the compressible steady flow around any Joukowski airfoil can be very efficiently obtained. In addition, the mean flow is obtained for arbitrary Φ_0 and Ψ_0, so that there is no restriction whatsoever on the particular grid that may be used for the unsteady calculation.

The only limitation in obtaining the mean potential flow by this particular approach is the underlying assumption that u_C and v_C must be small compared to U_∞. This means that the method will not give a good approximation in the inner region and particularly near the stagnation point where the perturbation velocities are of the same order of magnitude as U_∞. However, extensive testing of this particular approach and comparing with the steady potential flow solver FLO36 has shown that the region of inaccuracy is very small. Figures 1 through 4 show Mach number comparisons between the present approximate analytical scheme and FLO36. The comparison is made at grid points along fixed grid lines used by FLO36. It is seen that the agreement overall is quite good, with the

exception of grid points on the airfoil surface that are near the stagnation point. Because of this inaccuracy, we use FLO36 to calculate the mean flow quantities along the airfoil surface itself, and use the approximate analytical scheme off the airfoil except in a small region just upstream of the stagnation point. In this region, for airfoils that have steady loading, the velocities are calculated using a Taylor series expansion. For airfoils without steady loading, the velocities are calculated from a local analytical solution which is patched to the outer solution.

Frequency Domain Formulation

An inspection of equations (3.13), (3.14), (3.18), and (3.20) indicates that the time dependence of the present boundary value problem comes entirely through the harmonic term $e^{-ik_1 t}$. It is therefore possible to make a transformation from the time domain into the frequency domain by a simple change of dependent variable. By transforming the problem into the frequency domain, time is completely eliminated from the problem and it is possible to significantly simplify the mathematical formulation of the boundary value problem.

For the case of two-dimensional mean flow, we transform into the frequency domain by making the following change of dependent variable:

$$\phi_1 = \varphi e^{-ik_1 t + ik_3 x_3} \tag{3.34}$$

By including the $ik_3 x_3$ term in the transformation, the harmonic dependence on the spanwise component x_3 is also eliminated, since all of the $e^{ik_3 x_3}$ terms then factor out from each side of the equation. This is of course possible in view of (3.20) and (3.15).

Before presenting the governing equation in the new dependent variable φ, we introduce the linear operators $\mathcal{L}$ and $\mathcal{L}_0$ to simplify the notation.

$$\mathcal{L} = \frac{D_0}{Dt}\left(\frac{1}{{c_0}^2}\frac{D_0}{Dt}\right) - \frac{1}{\rho_0}\vec{\nabla}\cdot(\rho_0\vec{\nabla}) \tag{3.35}$$

and

$$\mathcal{L}_0 = M_\infty^2 \frac{D_0^2}{Dt_0^2} - \left(\frac{\partial^2}{\partial\Phi_0^2} + \frac{\partial^2}{\partial\Psi_0^2} + \frac{\partial^2}{\partial x_3^2}\right) \tag{3.36}$$

where

$$\frac{D_0}{Dt_0} = \frac{\partial}{\partial t} + \frac{\partial}{\partial\Phi_0} \tag{3.37}$$

The governing equation then takes the form

$$\mathcal{L}\phi_1 = \frac{1}{\rho_0}\vec{\nabla}\cdot(\rho_0\vec{u}^{(R)}) + \mathcal{L}\phi_2 \tag{3.38}$$

The operator $\mathcal{L}_0$ is essentially the operator for the linear thin airfoil gust response problem. By writing the governing equation in the following equivalent form, the left hand side of

the equation will exhibit the character of the thin airfoil operator in the far field since $\mathcal{L} \to \mathcal{L}_0$ there.

$$\mathcal{L}_0\phi_1 + (\mathcal{L} - \mathcal{L}_0)\phi_1 = \frac{1}{\rho_0}\vec{\nabla} \cdot (\rho_0 \vec{u}^{(R)}) + \mathcal{L}\phi_2 \tag{3.39}$$

We then have in terms of φ

$$\mathcal{L}_0\phi_1 + (\mathcal{L} - \mathcal{L}_0)\phi_1 =$$

$$e^{-ik_1 t + ik_3 x_3}\Big\{-[\beta_\infty^2 \frac{\partial^2 \varphi}{\partial \Phi_0^2} + \frac{\partial^2 \varphi}{\partial \Psi_0^2} + 2ik_1 M_\infty^2 \frac{\partial \varphi}{\partial \Phi_0} + (k_1^2 M_\infty^2 - k_3^2)\varphi]$$

$$+ [k_1^2 M_\infty^2 - \frac{k_1^2 M^2}{U_0^2} - ik_1 U_0^2 \frac{\partial}{\partial \Phi_0}(\frac{M^2}{U_0^2})]\varphi \tag{3.40}$$

$$+ [M^2(\frac{\partial U_0^2}{\partial \Phi_0} - 2ik_1) + 2ik_1 M_\infty^2 + U_0^4 \frac{\partial}{\partial \Phi_0}(\frac{M^2}{U_0^2}) - \frac{U_0^2}{\rho_0}\frac{\partial \rho_0}{\partial \Phi_0}]\frac{\partial \varphi}{\partial \Phi_0}$$

$$+ (\beta_\infty^2 - \beta^2 U_0^2)\frac{\partial^2 \varphi}{\partial \Phi_0^2} + (1 - U_0^2)\frac{\partial^2 \varphi}{\partial \Psi_0^2} - \frac{U_0^2}{\rho_0}\frac{\partial \rho_0}{\partial \Psi_0}\frac{\partial \varphi}{\partial \Psi_0}\Big\},$$

where M is the local Mach number of the mean flow.

Equation (3.40) may be simplified further by making the following change of both dependent and independent variables:

$$\varphi = \psi e^{-iK_0\Phi} \tag{3.41a}$$

where

$$K_0 = \frac{k_1 M_\infty^2}{\beta_\infty^2} \tag{3.41b}$$

and

$$\Phi = \Phi_0 \tag{3.42a}$$

$$\Psi = \beta_\infty \Psi_0 \tag{3.42b}$$

Expressing equation (3.40) in terms of ψ and the new independent variables Φ and Ψ, one gets

$$\mathcal{L}_0\phi_1 + (\mathcal{L} - \mathcal{L}_0)\phi_1 =$$

$$e^{-ik_1 t + ik_3 x_3} e^{-iK_0\Phi}\Big\{-\beta_\infty^2[\frac{\partial^2 \psi}{\partial \Phi^2} + \frac{\partial^2 \psi}{\partial \Psi^2} + (\frac{k_1^2 M_\infty^2}{\beta_\infty^4} - \frac{k_3^2}{\beta_\infty^2})\psi] \tag{3.43}$$

$$+ A_1\psi + A_2\frac{\partial \psi}{\partial \Phi} + A_3\frac{\partial \psi}{\partial \Psi} + A_4\frac{\partial^2 \psi}{\partial \Phi^2} + A_5\frac{\partial^2 \psi}{\partial \Psi^2}\Big\}$$

where $A_1 ... A_5$ are functions of (Φ, Ψ) defined by

$$A_1(\Phi,\Psi) = \frac{k_1^2 M_\infty^2}{\beta_\infty^2} - \frac{k_1^2 M^2}{U_0^2} - ik_1 U_0^2 \frac{\partial}{\partial \Phi}(\frac{M^2}{U_0^2}) \tag{3.44a}$$

$$- iK_0[M^2(\frac{\partial U_0^2}{\partial \Phi} - 2ik_1) + U_0^4 \frac{\partial}{\partial \Phi}(\frac{M^2}{U_0^2}) - \frac{U_0^2}{\rho_0}\frac{\partial \rho_0}{\partial \Phi}] + \frac{k_1^2 M_\infty^4}{\beta_\infty^4}\beta^2 U_0^2$$

$$A_2(\Phi,\Psi) = M^2(\frac{\partial U_0^2}{\partial \Phi} - 2ik_1) + U_0^4 \frac{\partial}{\partial \Phi}(\frac{M^2}{U_0^2}) - \frac{U_0^2}{\rho_0}\frac{\partial \rho_0}{\partial \Phi} + 2iK_0\beta^2 U_0^2 \tag{3.44b}$$

$$A_3(\Phi,\Psi) = -\frac{U_0^2}{\rho_0}\frac{\partial \rho_0}{\partial \Psi} \tag{3.44c}$$

$$A_4(\Phi,\Psi) = \beta_\infty^2 - \beta^2 U_0^2 \tag{3.44d}$$

$$A_5(\Phi,\Psi) = 1 - U_0^2 \tag{3.44e}$$

Note that in the far field the functions $A_1 ... A_5$ tend to zero so that the right hand side of (3.43) reduces to that of the linear thin airfoil theory.[12]

To complete the frequency domain formulation, it is necessary to present the right hand side of the governing equation (3.39). We will refer to the right hand side of (3.39) as the source term and denote it by $e^{-ik_1 t + ik_3 x_3} S$. To facilitate the presentation of the source term, we will write the governing equation as

$$\mathcal{L}_0\, \phi_1 + (\mathcal{L} - \mathcal{L}_0)\, \phi_1 = e^{-ik_1 t + ik_3 x_3}\, S \tag{3.45a}$$

or

$$\mathcal{L}_0\, \phi_1 + (\mathcal{L} - \mathcal{L}_0)\, \phi_1 = e^{-ik_1 t + ik_3 x_3}\, (S_1 + S_2 + S_3 - S_4) \tag{3.45b}$$

where

$$e^{-ik_1t+ik_3x_3}\ S_1 = \frac{\vec{\nabla}\rho_0}{\rho_0}\cdot\{[\vec{\nabla}(\vec{a}\cdot\vec{X})]e^{i\vec{k}\cdot\vec{X}-ik_1t}+\vec{\nabla}\tilde{\phi}\} \tag{3.46a}$$

$$e^{-ik_1t+ik_3x_3}\ S_2 = \vec{\nabla}\cdot\{[\vec{\nabla}(\vec{a}\cdot\vec{X})]e^{i\vec{k}\cdot\vec{X}-ik_1t}+\vec{\nabla}\tilde{\phi}\} \tag{3.46b}$$

$$e^{-ik_1t+ik_3x_3}\ S_3 = \frac{D_0}{Dt}(\frac{1}{{c_0}^2}\frac{D_0\phi_2}{Dt}) \tag{3.46c}$$

$$e^{-ik_1t+ik_3x_3}\ S_4 = \frac{1}{\rho_0}\vec{\nabla}\cdot(\rho_0\vec{\nabla}\phi_2) \tag{3.46d}$$

The frequency domain governing equation is then given by

$$\begin{aligned} &-\beta_\infty^2[\frac{\partial^2\psi}{\partial\Phi^2}+\frac{\partial^2\psi}{\partial\Psi^2}+(\frac{k_1^2M_\infty^2}{\beta_\infty^4}-\frac{k_3^2}{\beta_\infty^2})\psi] \\ &+A_1\psi+A_2\frac{\partial\psi}{\partial\Phi}+A_3\frac{\partial\psi}{\partial\Psi}+A_4\frac{\partial^2\psi}{\partial\Phi^2}+A_5\frac{\partial^2\psi}{\partial\Psi^2} \\ &=e^{iK_0\Phi}(S_1+S_2+S_3-S_4) \end{aligned} \tag{3.47}$$

where $A_1...A_5$ are defined by equations (3.44) and $S_1...S_4$ are defined by equations (3.46). In the far field both the coefficients $A_1...A_5$ and the source term $S_1+S_2+S_3-S_4$ tend to zero so that the equation reduces to a Helmholtz equation.

We conclude this section by presenting the frequency domain formulation of the airfoil and wake boundary conditions given by equations (3.10), (3.11a) and (3.11b). In terms of the new coordinates (Φ,Ψ) and the new dependent variable ψ, equation (3.10) for the airfoil boundary condition becomes

$$\frac{\partial\psi}{\partial\Psi}=-\frac{e^{iK_0\Phi}}{\beta_\infty}[\frac{a_1\beta_\infty\Gamma}{\pi}\ \frac{1-e^{-\Phi^2}}{\Phi}\ +\ \frac{a_2+ia_0a_1k_2}{1+ia_0k_1}]e^{ik_1X_{e,1}}. \tag{3.48}$$

The wake boundary condition (3.11a) becomes

$$(-ik_1\ +\ U_0^2\frac{\partial}{\partial\Phi})[\triangle(\psi e^{-iK_0\Phi}\ -\ \varphi_2)]=0, \tag{3.49a}$$

where

$$e^{-ik_1t+ik_3x_3}\ \varphi_2\ =\ \phi_2 \tag{3.49b}$$

and where $\triangle(\psi e^{-iK_0\Phi} - \varphi_2)$ denotes the jump in the quantity $(\psi e^{-iK_0\Phi} - \varphi_2)$ across the vortex sheet behind the airfoil. Finally, condition (3.11b) becomes

$$\triangle[\vec{\nabla}(\psi e^{-iK_0\Phi} - \varphi_2) \cdot \vec{n}] = 0. \tag{3.49c}$$

Transformation into Computational Coordinates and Formulation of the Numerical Boundary Value Problem

Our basic numerical approach to solving equation (3.47) is to use the method of finite difference approximations. By discretizing the flow field and employing finite differences at each grid point, a large linear system of equations is obtained which can be solved using a matrix solver.

Previous experience in solving equation (3.47) for the case of flat plate and symmetric airfoils has shown that the independent variables (Φ, Ψ) are not suitable computational coordinates for the gust response problem.[10,11] There are difficulties in obtaining consistently accurate results over a large range of Mach numbers and reduced frequencies, and also problems with the implementation of far field boundary conditions. A transformation of the independent variables is needed which not only provides an adequate distribution of grid points around the airfoil in the near field, but also provides a distribution of grid points in the far field which is suitable for acoustic wave propagation and the implementation of far field, radiation type boundary conditions.

In order to satisfy these requirements, we make a transformation into the elliptic coordinates (η, ξ) with the transformation

$$\Phi = a^\star \cos(\pi\eta)\cosh(\pi\xi) \tag{3.50a}$$

$$\Psi = a^\star \sin(\pi\eta)\sinh(\pi\xi). \tag{3.50b}$$

where $a^\star$ is an arbitrary constant which will be defined later. Note that in the far field the elliptic coordinates reduce essentially to cylindrical coordinates, and that the $\Phi - \Psi$ plane is mapped into a semi-infinite strip in the $\eta - \xi$ plane.

With this change of variables, the governing equation takes the following form:

$$\begin{aligned}
&-\beta_\infty^2\left[\frac{\partial^2\psi}{\partial\eta^2} + \frac{\partial^2\psi}{\partial\xi^2} + J(\eta,\xi)\left(\frac{k_1^2 M_\infty^2}{\beta_\infty^4} - \frac{k_3^2}{\beta_\infty^2}\right)\psi\right] \\
&+ A_1\, J(\eta,\xi)\,\psi + T_1\frac{\partial\psi}{\partial\xi} + T_2\frac{\partial\psi}{\partial\eta} + T_3\frac{\partial^2\psi}{\partial\xi^2} + T_4\frac{\partial^2\psi}{\partial\eta^2} + T_5\frac{\partial^2\psi}{\partial\eta\partial\xi} \\
&= e^{iK_0\Phi}(S_1 + S_2 + S_3 - S_4)\, J(\eta,\xi).
\end{aligned} \tag{3.51}$$

Here $J(\eta,\xi)$ is the Jacobian of the transformation (3.50) which is given by

$$J(\eta,\xi) = \pi^2 a^{\star 2}[\sin^2(\pi\eta) + \sinh^2(\pi\xi)]\,, \tag{3.52}$$

and the T_i coefficients are known functions of η and ξ.

The airfoil boundary condition (3.48) has also been transformed through the change of variables (3.50). Expressing condition (3.48) in the variables (η,ξ), one gets

$$\frac{\partial\psi}{\partial\xi} = -a^\star\pi\,\sin(\pi\eta)\,\frac{e^{iK_0\Phi}}{\beta_\infty}\,[\,\frac{a_1\beta_\infty\Gamma}{\pi}\,\frac{1-e^{-\Phi^2}}{\Phi} + \frac{a_2+ia_0a_1k_2}{1+ia_0k_1}\,]e^{ik_1X_{e,1}}. \tag{3.53}$$

We now proceed to discuss the remaining boundary conditions. First, the wake boundary condition (3.49a) may be integrated so that it becomes

$$\triangle(\psi e^{-iK_0\Phi}) = \triangle\varphi_2 + [\triangle(\psi e^{-iK_0\Phi})_{t.e.} - \triangle\varphi_{2\,t.e.}]e^{ik_1\int_{\Phi_{t.e.}}^{\Phi}\frac{d\Phi}{U_0^2}}, \tag{3.54}$$

where the subscript $t.e.$ denotes quantities at the airfoil trailing edge. Note that, in general, both ψ and Φ are discontinuous across the wake, so that in evaluating $\triangle(\psi e^{-iK_0\Phi})$, it is necessary to take into account the jump in both ψ and Φ. This condition is imposed for grid points on the lower side of the wake.

On the upper side of the wake, we impose condition (3.49c), which specifies that the normal velocity component of the unsteady velocity is continuous across the wake. This may be written

$$\Big[U_0\,\frac{\partial}{\partial\Psi}(\psi e^{-iK_0\Phi} - \varphi_2)\Big]^+ = \Big[U_0\,\frac{\partial}{\partial\Psi}(\psi e^{-iK_0\Phi} - \varphi_2)\Big]^- \tag{3.55}$$

where "+" and "−" superscripts denote above and below the wake, respectively, and the derivatives in (3.55) are taken to be one-sided.

In order to proceed further in the development of the boundary conditions (3.54) and (3.55) in terms of the computational coordinates (η,ξ), it is necessary to first discuss in more detail the transformation (3.50). First, the constant $a^\star$ is determined from the condition that the airfoil trailing edge point on the suction side, where $\Phi = a^\star, \Psi = 0$, should map into the point $\eta = 0, \xi = 0$, and the stagnation point, where $\Phi = -a^\star, \Psi = 0$ should map into the point $\eta = 1, \xi = 0$. Then $a^\star$ must be determined from

$$a^\star = \frac{1}{2}\int_{t.e.}^{s.p} U_0\,ds \tag{3.56}$$

where s denotes the arc length along the airfoil surface, $t.e.$ denotes the airfoil trailing edge, and $s.p.$ denotes the stagnation point. The steady solver FLO36 is used to locate the stagnation point, and the integration in (3.56) is carried out using trapezoidal integration.

The suction surface of the airfoil, then, corresponds to the line segment on the η axis between 0 and 1, and the pressure surface corresponds to the line segment on the η axis between 1 and $\eta_{t.e.-}$, where $\eta_{t.e.-} < 2.0$ (See Figure 5.) The pressure side of the wake then corresponds to the line segments given by $\{\eta_{t.e.-} < \eta \leq 2.0,\ \xi = 0\}$, and $\{\eta = 2.0,\ \xi > 0\}$. The suction side of the wake corresponds to the positive ξ axis. The upper boundary of the $\eta - \xi$ grid, which is given by $\{\xi = \xi_{max},\ 0 \leq \eta \leq 2\}$, corresponds to the far field boundary in the $\Phi - \Psi$ plane.

Because of the discontinuity in Φ across the wake grid line, the grid points on the upper and lower sides of the wake in the physical plane (the $x_1 - x_2$ plane) do not coincide. This presents some difficulty in the implementation of boundary conditions (3.54) and (3.55), inasmuch as these conditions both specify a relation that must be satisfied across the wake. The difficulty can be removed, however, by simply using a linear averaging of ψ at the two adjacent grid points to represent ψ at an arbitrary point in between. Using such a linear averaging, then, boundary condition (3.54), which is imposed for wake grid points on the pressure side, becomes

$$\left[(\psi e^{-iK_0\Phi})\right]^+_{avg} - \left[(\psi e^{-iK_0\Phi})\right]^-$$

$$= \Delta\varphi_2 + [\Delta(\psi e^{-iK_0\Phi})_{t.e.} - \Delta\varphi_{2t.e.}]e^{ik_1\int_{\Phi_{t.e.}}^{\Phi}\frac{d\Phi}{U_0^2}}. \tag{3.57}$$

The discontinuity in Φ across the wake also leads to a shift in the location of the corresponding grid points in the physical plane on opposite sides of the wake. Because of this shift, the last several grid points on the pressure side in the physical plane extend past the last suction side wake grid point, so that the above averaging technique cannot be employed. (See Figure 5) However, because these last few points are in the far field where the mean flow is nearly uniform, the function ψ behaves essentially as in the case of the thin airfoil problem, and is approximately an odd function of Ψ. By assuming ψ to be an odd function with respect to Ψ in the far field, condition (3.54) becomes

$$\left[(\psi e^{-iK_0\Phi})\right]^- = -\frac{1}{2}\Delta\varphi_2 - \frac{1}{2}[\Delta(\psi e^{-iK_0\Phi})_{t.e.} - \Delta\varphi_{2t.e.}]e^{ik_1\int_{\Phi_{t.e.}}^{\Phi}\frac{d\Phi}{U_0^2}} \tag{3.58}$$

for extra far field wake grid points on the pressure side.

For wake grid points on the suction side, the linear averaging technique can be used for all points, and condition (3.55) becomes

$$\left[U_0\frac{\partial}{\partial\Psi}(\psi e^{-iK_0\Phi} - \varphi_2)\right]^+ = \left[U_0\frac{\partial}{\partial\Psi}(\psi e^{-iK_0\Phi} - \varphi_2)\right]^-_{avg}. \tag{3.59}$$

Expressing this in η and ξ, one gets

$$\left[e^{-iK_0\Phi}\frac{U_0}{\sinh(\pi\xi)}\frac{\partial\psi}{\partial\eta}\right]^+ - \left[e^{-iK_0\Phi}\frac{U_0}{\sin(\pi\eta)}\frac{\partial\psi}{\partial\xi}\right]^-_{avg}$$

$$= U_0^+\left(\frac{\partial\varphi_2^+}{\partial\Psi} - \frac{\partial\varphi_2^-}{\partial\Psi}\right) \tag{3.60}$$

when the averaged values of ψ lie on the η axis. When the averaged values of ψ lie on the right hand boundary of the $\eta-\xi$ grid $\{\eta = 2.0,\ \xi > 0\}$, (3.59) becomes

$$\left[e^{-iK_0\Phi}\frac{U_0}{\sinh(\pi\xi)}\frac{\partial\psi}{\partial\eta}\right]^+ - \left[e^{-iK_0\Phi}\frac{U_0}{\sinh(\pi\xi)}\frac{\partial\psi}{\partial\eta}\right]^-_{avg}$$

$$= U_0^+\left(\frac{\partial\varphi_2^+}{\partial\Psi} - \frac{\partial\varphi_2^-}{\partial\Psi}\right) \tag{3.61}$$

In order to complete the formulation of the boundary conditions, it is only necessary to specify conditions at the airfoil trailing edge and in the far field. At the trailing edge, there are two grid points that coincide, one corresponding to the suction side of the airfoil and one corresponding to the pressure side. It is therefore necessary to impose two conditions at the trailing edge point. At the point on the suction side, which corresponds to $(\eta,\xi) = (0,0)$, the Jacobian of the coordinate transformation (3.50) vanishes. Since the Kutta condition requires that the velocity at the trailing edge be finite, we are led to the requirement that

$$\frac{\partial\psi}{\partial\eta} = 0 \quad \text{at} \quad (\eta,\xi) = (0,0). \tag{3.62}$$

At the pressure side trailing edge point, we impose the condition that the unsteady pressure is continuous,

$$p'_{t.e.+} = p'_{t.e.-} \quad \text{at} \quad (\eta,\xi) = (\eta_{t.e.-},0). \tag{3.63}$$

We point out that since the Jacobian vanishes at the suction side trailing edge point, it is not possible to directly calculate the pressure in $\eta-\xi$ coordinates at that point. However, it can be calculated using a Taylor series expansion from neighboring points. By using this approach, condition (3.63) can be satisfied.

In presenting the far field boundary condition, we first comment that while condition (3.12) expresses the mathematical requirement that $\vec{\nabla}\phi_1 \to 0$ at upstream infinity, this condition cannot be imposed throughout the far field on a boundary at a finite distance from the airfoil. To implement such a condition would impose a reflecting boundary condition which can lead to large errors in the solution.

To correctly model the physics of the present unsteady boundary value problem requires that the far field boundary condition be such that it allows outgoing acoustic waves to leave the solution domain without being reflected back into the computational grid. This can be accomplished, for example, by using separation of variables along with a series expansion for the far field solution ψ and only accepting those terms in the series which represent outgoing waves. The difficulty with this approach, however, is that it leads to a matrix which requires pivoting and therefore longer solution times. In addition, since ψ is not continuous across the wake, but the series expansion for ψ is continuous everywhere, there is an incompatibility near the wake which can lead to a poor solution in the far field.

An alternative to the series expansion approach is to use a Sommerfield radiation condition on the unsteady pressure. This approach avoids both the difficulties associated with the series expansion method and is also easier to implement. The Sommerfield radiation condition for the pressure is the approach used in the present work, and may be written in operator notation as

$$\Big[\frac{\partial}{\partial R} - i\sqrt{(\frac{k_1 M_\infty}{\beta_\infty^2})^2 - (\frac{k_3}{\beta_\infty})^2}\Big](\frac{\partial}{\partial \Phi} - i\frac{k_1}{\beta_\infty^2})\,\psi = 0 \tag{3.64}$$

where

$$\Phi = R\cos\Theta \tag{3.65a}$$

$$\Psi = R\sin\Theta. \tag{3.65b}$$

Neglecting $\frac{1}{R}\frac{\partial}{\partial\Theta}$ terms, this reduces to

$$\cos\Theta\frac{\partial^2\psi}{\partial R^2} - i\Big[\sqrt{(\frac{k_1 M_\infty}{\beta_\infty^2})^2 - (\frac{k_3}{\beta_\infty})^2}\cos\Theta + \frac{k_1}{\beta_\infty^2}\Big]\frac{\partial\psi}{\partial R}$$

$$- \frac{k_1}{\beta_\infty^2}\Big[\sqrt{(\frac{k_1 M_\infty}{\beta_\infty^2})^2 - (\frac{k_3}{\beta_\infty})^2}\Big]\,\psi = 0 \tag{3.66}$$

This condition is applied for all grid points such that $0 < \eta < 2$, $\xi = \xi_{\max}$.

Numerical Method

In the previous section we presented the transformation into computational coordinates and the development of the numerical boundary value problem. The problem to be solved numerically consists of the governing equation (3.51), and the boundary conditions (3.53), (3.57), (3.58), (3.60), (3.61), (3.62), (3.63) and (3.66). As mentioned previously, our basic numerical approach is to use the method of finite difference approximations, and then to solve the resulting linear system of equations using a matrix solver.

The first step in obtaining numerical solutions to equation (3.51) and its associated boundary conditions for a given flow configuration is to calculate the source term S and the coefficient functions $A_1 ... A_5$. This requires the evaluation of Lighthill's drift function and its first and second partial derivatives with respect to Ψ, and the evaluation of the mean flow quantities and their partial derivatives with respect to Φ and Ψ at each interior grid point. The mean flow quantities are obtained through the analytical scheme presented previously in the present paper, and their derivatives are calculated using four point differencing.

It should be emphasized that accurate evaluation of the source term is essential if accurate solutions to equation (3.51) are to be obtained, and this in turn depends largley upon the accurate evaluation of the drift function. If the drift function is not evaluated accurately, then the source term will not tend to zero in the far field and the numerical scheme will become unstable. One of the major advantages of using the analytical scheme outlined previously in this section to obtain the mean flow is that it can determine the mean velocities at arbitrary (Φ, Ψ). This means that for fixed Ψ, i.e. on a given streamline, we can determine the mean velocities for arbitrary Φ. Since evaluation of the drift function requires the integration of the expression $(\frac{1}{U_0^2} - \frac{1}{U_\infty^2})$ with respect to Φ on a fixed streamline, it is very easy to do the numerical integrations necessary to accurately evaluate the drift function Δ. In the actual calculations, we evaluate Δ at a given grid point as the sum of an analytically determined part and a numerically determined part. The analytical part comes from a far field expansion for Δ which is given by

$$\Delta = \Phi_0 - \frac{\Gamma}{\pi}\mathrm{sgn}(\Psi_0)\Big[\frac{\pi}{2} + \mathrm{sgn}(\Psi_0)\tan^{-1}(\frac{\Phi_0}{\beta_\infty \Psi_0})\Big] \tag{3.67}$$

This expression can be used to accurately calculate Δ at some point far upstream, and then since Δ is additive, the remaining portion of the integration can be done numerically from the upstream location to the given grid point. The numerical integration is done using the trapezoid rule with variable spacing in Φ to ensure accurate resolution near the airfoil. The first and second partial derivatives of Δ are approximated using four point differencing.

Once S and $A_1 ... A_5$ have been calculated, they can be stored separately and passed to the subroutine which sets up the matrix equation to be solved.

We now proceed to discuss the differencing used for the governing equation and boundary conditions. To represent equation (3.51) we use the standard nine-point, central difference computational molecule which is second order accurate in η and ξ. We assume in general that the spacing in each direction is nonuniform. Details of the grid spacing will be discussed momentarily. Each of the boundary conditions (3.53), (3.62), (3.63), and (3.66) are implemented using four-point, one-sided differencing which is third order accurate for (3.53), (3.62), and (3.63), and second order accurate for (3.66). Boundary conditions (3.60) and (3.61) are both implemented using three-point, one-sided differencing which is second order accurate.

Obtaining a numerical solution to the finite difference equations representing the governing equation (3.51) and its associated boundary conditions requires solving a large

matrix equation whose size is equal to twice the number of grid points. There are difficulties in solving this linear system of equations because the matrix is not block tridiagonal and does not have a regular block structure which can be exploited. In addition, iterative solvers have convergence problems because the diagonal dominance of the matrix changes as the parameters M_∞, k_1, and k_3 are varied.

Because of these difficulties, a general purpose sparse matrix solver was developed which stores only the nonzero entries of the matrix and can solve an arbitrary sparse matrix equation using Gaussian elimination. The solver basically works by using an ordered list to represent the nonzero entries of each row in the matrix, and then inserts and deletes new entries in the rows of the matrix as multiples of each row are added to other rows to carry out the elimination process. The only requirement for the solver to work is that the matrix must be arranged such that it remains reasonably sparse during the elimination procedure.

The sparse solver has both a pivoting and non-pivoting feature. However, as pivoting during the elimination process proved to be unnecessary, the pivoting feature was not used. By not pivoting during the elimination, it was possible to increase the storage efficiency of the solver and thereby solve larger systems of equations. The increased storage efficiency was gained by using a mapping function to map sub-blocks of the rectangular two-dimensional arrays containing the nonzero entries of the matrix and their associated column numbers into singly dimensioned arrays which contained less unused storage. By using this technique, the storage efficiency of the solver was increased by about 25 percent.

The final issue to be discussed in regard to our numerical scheme is the method of grid determination. As reported previously,[10,11] it is not possible to use a single grid and obtain accurate solutions to the gust response problem for a large range of reduced frequencies. Rather, the unsteady grid must be determined as a function of both the mean flow Mach number and the reduced frequency.

This requirement is dictated by both the accuracy of the far field boundary condition (3.66), and the need to adequately model the airfoil boundary condition (3.56) and the wake boundary conditions (3.57) and (3.58). The accuracy of the far field boundary condition depends on the reduced frequency k_1 and free stream Mach number M_∞ in such a way that the parameter $\frac{k_1 M_\infty}{\beta_\infty^2} R$, where R is the distance to the far field boundary, should remain at least $O(1)$. This shows that the location of the outer boundary of the grid must be determined as a function of k_1 and M_∞. In addition, there should be enough grid points per wavelength to accurately represent the airfoil and wake boundary conditions. Due to the harmonic terms containing the parameters K_0 and k_1, this shows that the η and ξ spacing have to be determined as a function of k_1 and M_∞.

The spacing in the η direction is constant for $0 \leq \eta \leq 1$, and then changes slightly but constant again for $1 \leq \eta \leq \eta_{t.e.-}$, and finally constant again, but slightly different from the two previous intervals, for $\eta_{t.e.-} \leq \eta \leq 2$. The spacing on $0 \leq \eta \leq \eta_{t.e.-}$ determines the spacing on the airfoil surface. Normally the number of grid points in the η direction varies from 40 for the low frequencies up to about 70 for reduced frequencies of 4.

An optimal spacing of the grid points in the wake (the ξ direction) turns out to be more difficult to achieve than the spacing on the airfoil. Numerical studies of the thin airfoil gust response problem showed that the optimal choice of spacing was 12 uniformly spaced grid points per wavelength. For the case of the thin airfoil, the wake boundary condition analogous to condition (3.57) is much simpler, and it is possible to choose the spacing of the ξ grid points such that they are uniformly spaced along the waves. However, for the general problem of nonuniform mean flows, the waves in the wake are distorted due to the $e^{ik_1 \int_{\Phi_{t.e.}}^{\Phi} \frac{d\Phi}{U_0^2}}$ term, and it is no longer possible to determine the grid point spacing such that they are uniformly spaced along the waves. This does not prove to be a difficulty, however, because in the far field the general problem of vortical flows past a lifting airfoil reduces essentially to a linear problem as the mean flow tends to become uniform. So we may determine the wake spacing as in the case of the flat plate airfoil, and in the far field the grid points will be nearly uniformly spaced along the waves.

For a flat plate airfoil, the wake boundary condition which imposes the continuity of the pressure is given, corresponding to the transformation (3.50), by

$$\psi_{wake,j} = \psi_{t.e.} e^{i\frac{k_1}{\beta_\infty^2}[a^\star \cosh(\pi\xi_j) - a^\star]}. \tag{3.68}$$

In order to have uniformly spaced grid points along the waves in the wake, the argument of the exponential function should vary by equal fractional increments of π. To place 12 grid points per wavelength, we are then led to the requirement that the location of the $j\,th$ ξ grid point be determined from the relation

$$\frac{k_1}{\beta_\infty^2}[a^\star \cosh(\pi\xi_j) - a^\star] \;=\; j\,\frac{2\pi}{12}. \tag{3.69}$$

Solving for ξ_j, we get

$$\xi_j = \frac{1}{\pi}\cosh^{-1}\Big(j\,\frac{\pi\beta_\infty^2}{6a^\star k_1} + 1\Big). \tag{3.70}$$

This is the method for determining the ξ spacing in the far field. Near the airfoil the above procedure leads to a spacing which is too coarse to be used. So near the airfoil we use uniform ξ spacing which remains constant at some value $\Delta\xi$, until a point is reached such that the ξ_j determined from (3.70) satisfy $\xi_{j+1} - \xi_j \leq \Delta\xi$. From that point on, the spacing of the ξ grid points is determined from (3.70).

IV. CODE VALIDATION

Extensive efforts were taken to validate the computer codes which were developed to implement the numerical solution procedure which was outlined in the previous section. The validation process consisted of a combination of comparing numerical results with known analytical solutions to the classical thin airfoil gust response problems, comparing

with the second order theory of Goldstein and Atassi[3] and Atassi,[4] comparing with the first order numerical results of Atassi and Grzedzinski,[13] and calculating solutions to limiting case problems i.e., as Mach number, thickness, angle of attack, or camber go to zero.

Sample computation times for the results presented varied considerably, depending on the reduced frequency, Mach number, and airfoil loading. For thin, unloaded airfoils, with low reduced frequency gusts, typical solution times were about 20 seconds per frequency on the Cray X-MP at the NASA Lewis Research Center. The higher frequencies for these airfoils required on the order of 60 CPU seconds per frequency, with slightly higher solution times as the Mach number increases. For thick, symmetric, unloaded airfoils, the solution times range from about 40 seconds for the lower frequencies up to about 150 seconds for the highest frequencies. Finally, for loaded airfoils, the solution times ranged from about 250 seconds for the low frequencies up to around 1200 seconds for the highest reduced frequencies. No effort was made to optimize the computational efficiency of the scheme, as our main purpose was to validate its accuracy.

In the results that follow, comparisons are made for one-dimensional (transverse) gusts, two-dimensional (transverse and longitudinal) gusts, and fully three-dimensional gusts. See Figures 6, 7, and 8.

The first step in the validation process was to compare numerical results with known solutions to the classical thin airfoil gust response problems. In Figures 9 and 10 we present comparisons between numerical and analytical results for the normalized unsteady lift for vortical flows past flat plate airfoils with zero thickness. The normalized unsteady lift, commonly called the response function, is defined by

$$R_L(k_1, k_3, M_\infty) = \frac{L'}{\pi \rho_\infty c U_\infty |\vec{a}| e^{i\omega t}} \tag{4.1}$$

where L' is the unsteady lift. Figure 9.a shows a comparison between numerical results and the Sears solution[14] for the case of a one-dimensional (transverse) gust in incompressible flow, and Figures 9.b and 9.c compare numerical results and analytical results obtained from a Possio solver for a one-dimensional gust at Mach numbers of .5 and .8. The reduced frequency values at which the comparisons are made range from 0 to 4.0, and are shown below the plot. The point on the real axis and furthest to the right corresponds to $k_1 = 0$, and the other points along the curve correspond in order to the other reduced frequency values. Figures 10.a through 10.c compare numerical results and analytical results from a Possio solver for three-dimensional gusts for Mach numbers of .1, .5, and .8. The conditions on the gust wave number parameters are shown below the plots. As can be readily seen, there is excellent agreement between the numerical and analytical results. The only loss of accuracy occurs when both the Mach number and reduced frequency become large.

In order to assess the accuracy of the present numerical scheme for vortical flows around thin airfoils in which the mean flow is not uniform, we compare with the second order theory of Goldstein and Atassi [3] and Atassi.[4] The results given by Atassi assume a zero thickness airfoil, but account for the effects of airfoil camber and angle of attack on the

airfoil unsteady response. In Figure 11, we compare the numerically computed response function with the second order theory for an incompressible flow with a two-dimensional gust about an airfoil with an angle of attack of two degrees and a camber ratio of .05. The numerically computed response function is for a 6% thick Joukowski airfoil, while the second order theory does not take into account the airfoil thickness. The reduced frequency values used for the comparison are shown below the plot. As can be seen, the numerical results for the 6% thick airfoil show a slightly larger lift at the low frequencies, but a slightly smaller lift at the higher frequencies for k_1 up to about 3.0. As shown in the results presented in [5] and [15], this effect can be attributed entirely to the thickness of the airfoil, so that the agreement is very good for reduced frequencies ranging from 0 up to about 3.0. For the frequencies higher than 3.0, it is not possible to make any firm conclusion on the accuracy of the numerical results.

To validate the numerical scheme for airfoils with thickness, we compare with the results of Atassi and Grzedzinski.[13] In Figure 12, we show comparisons for one-, two-, and three-dimensional gusts for incompressible flows around a 12% thick Joukowski airfoil with zero degrees angle of attack and zero camber ratio. The reduced frequency values for the comparison range from .2 to 2.5 and are shown on the plots. We limit the comparison to this range of k_1, since this is roughly the range of validity of the Green's function approach of Atassi and Grzedzinski. The agreement between the two sets of results is good in general.

The final step in the validation process was to calculate the solutions to various limiting case problems. The limiting case of $M_\infty \to 0$, i.e., the incompressible case, was covered above where the numerical results were compared to the Sears solution. We now present results for the limiting cases of airfoil thickness, angle of attack, and camber.

In Figures 13 through 16, we compare numerical results for the unsteady lift and moment about the airfoil center of a 3% thick, symmetric Joukowski airfoil with that of a flat plate airfoil with zero thickness. Analogous to the response function R_L for the unsteady lift, we define the response function R_M for the unsteady moment by

$$R_M(k_1, k_3, M_\infty) = \frac{M'}{\frac{\pi}{2}\rho_\infty c^2 U_\infty |\vec{a}| e^{i\omega t}} \tag{4.2}$$

where M' is the unsteady moment about the airfoil center. Figures 13 and 14 present results for $M_\infty = .1$, and Figures 15 and 16 present results for $M_\infty = .6$. For both Mach numbers, it is seen that the small airfoil thickness has little effect on the unsteady response, except for high reduced frequencies in the two-dimensional gust case, where the magnitude of the unsteady lift is reduced by 15 - 20 percent. It would appear from these results that thickness effects become more important at the higher frequencies for the case of the two-dimensional gust.

Figures 17 and 18 present comparisons between results for a 12% thick symmetric Joukowski airfoil at zero degrees angle of attack and one degree angle of attack. All plots are for a free stream Mach number of .1. As in the case of airfoil thickness, the strongest

effect is seen in the two-dimensional gust case. However, here there is a significant effect both for the low and high reduced frequencies. At the low frequency end, the effect is primarily a reduction in the magnitude of the unsteady lift, while at the high end it is primarily a change in phase of the unsteady lift. We also point out that, in agreement with the theoretical results of Atassi,[4] for the transverse gust case in which the gust has only an upwash component, the steady loading on the airfoil has virtually no effect on the unsteady lift.

Finally, in Figures 19 through 20, we compare results for a 12% thick Joukowski airfoil with no camber with a 12% thick Joukowski airfoil with a camber ratio of .02. The free stream Mach number for all plots is .1, and the angle of attack is zero degrees. The effect here is exactly analogous to the effect of small angle of attack, except that it is stronger in this case due to the increased steady loading on the airfoil. For the one degree angle of attack airfoil the steady lift coefficient was .12, while for the 2% cambered airfoil the steady lift coefficient was .27. In each case, the reduction of the quasi-steady lift ($k_1 = 0 = k_2$) for the two-dimensional gust is directly proportional to the steady loading on the airfoil with a proportionality constant of 0.26. Using the theoretical results of Atassi reported in [4], it can be shown that for zero thickness airfoils in a two-dimensional gust in incompressible flow, the reduction in the quasi-steady lift for airfoils with small camber and angle of attack is proportional to the steady lift coefficient with a proportionality constant of $\frac{1}{\pi}\frac{k_2}{|k|}$ = .23. The difference between the numerical and theoretical values of the proportionality constant can be accounted for by the fact that the theoretical result does not account for the thickness of the airfoil, and also assumes a parabolic profile for the airfoil camber line.

In Reference 15 a more general study of how the two-dimensional quasi-steady lift changes in response to mean airfoil loading showed that for airfoils with heavier loading and Mach number effects the value of the proportionality constant was about .25. We thus conclude that the reduction in the two-dimensional quasi-steady lift due to mean airfoil loading is roughly proportional to the steady lift coefficient of the loaded airfoil with a proportionality constant of .25.

Before concluding the discussion of numerical results, the authors would like to emphasize the significance of the method of grid determination which was outlined in the previous section. In Figure 21 we present numerical results which demonstrate the kinds of errors that can occur as a result of using an inappropriate grid. The results shown in these figures were generated without determining the grid as a function of the reduced frequency. For each case shown, the same grid was used for all frequencies in the calculation. The grid used for each Mach number was the one normally used only for the highest reduced frequency. By using the grid for the highest frequency, it was assured that there would be sufficient grid resolution to resolve the waves for the lower frequencies. But as can be seen, the agreement is not nearly as good as when the grid is determined as a function of both the Mach number and reduced frequency. These results show the effect of keeping the outer boundary fixed, and not varying it with the reduced frequency in order to ensure that the representation of the far field boundary condition is sufficiently accurate.

The results in Figure 22 show the kinds of errors that can occur when the grid points are not suitably spaced in the far field. The grids used for the results in Figure 22 used an exponentially decreasing spacing which was varied to ensure that there were enough grid points per wavelength to adequately model the wavelike structure of the solution. In addition, the location of the far field boundary was also varied to ensure that the far field boundary condition would be sufficiently accurate. However, as the results show, there are large errors in the response function curves. This is due to the fact that exponential spacing is not suitable for this kind of wave propagation problem.

V. CONCLUSION

In the present paper the authors have presented a finite-difference, frequency-domain numerical scheme for the solution of unsteady, subsonic vortical flows around lifting airfoils. The present method is an alternative to the potential and primitive variable methods, and due to its inherent efficiency and ability to correctly handle the convection and distortion of the upstream vorticity by the nonuniform mean flow, represents an ideal solution method for unsteady aerodynamic flow fields.

The computer codes that have been developed to implement the present numerical approach have been validated through extensive comparisons with known solutions to unsteady vortical flow problems and through the calculation of various limiting case problems. The numerical results have shown that our numerical scheme can calculate with very good accuracy the solutions to a large variety of unsteady vortical flow problems. We conclude that for symmetric airfoils and loaded airfoils with small mean loading, the present scheme is very accurate for reduced frequencies ranging from 0 up to at least 4.0, for both incompressible and compressible flows. For more heavily loaded airfoils, the scheme has similar accuracy for reduced frequencies ranging from 0 up to around 3.0. For reduced frequencies above 3.0, it is not possible to make any firm conclusion on the accuracy of the present numerical scheme for airfoils with substantial mean loading. This is an area that requires further study.

Among the most important features of our numerical approach are the transformation of the independent variables into elliptic coordinates, the method of determining the unsteady grid as a function of the Mach number and reduced frequency, the far field radiation condition for the unsteady pressure, the general purpose direct sparse matrix solver, and the formulation and method of evaluation of the source term.

Finally, the authors are in the process of extending the present linearized unsteady aerodynamic analysis and numerical solution procedure to include transonic flows. Details will be presented in a future paper.

REFERENCES

1. McCroskey, W.J. and Goorjian, P.M., "Interactions of Airfoils with Gusts and Concentrated Vortices in Unsteady Transonic Flow," AIAA Paper 83-1691, July 1983.
2. McCroskey, W. J., "The Effects of Gusts on the Fluctuating Airloads of Airfoils in Transonic Flow," *Journal of Aircraft,* Vol. 22, No. 3, March 1985, pp. 236-243.
3. Goldstein, M. E. and Atassi, H. M., "A Complete Second-Order Theory for the Unsteady Flow About an Airfoil Due to a Periodic Gust," *J. Fluid Mech.,* Vol. 74, 1976, pp. 741-765.
4. Atassi, H.M., "The Sears Problem for a Lifting Airfoil Revisited - New Results," *J. Fluid Mech.* Vol. 141, 1984, pp. 109-122.
5. Scott, J.R. and Atassi, H.M., "Numerical Solutions of the Linearized Euler Equations for Unsteady Vortical Flows Around Lifting Airfoils," AIAA Paper 90-0694, January 1990.
6. Lighthill, M.J., "Drift" *J. Fluid Mech.,* Vol. 1, 1956, pp. 31-53.
7. Goldstein, M. E., "Unsteady Vortical and Entropic Distortions of Potential Flows Round Arbitrary Obstacles," *J. Fluid Mech.,* Vol. 89, 1978, pp. 433-468.
8. Atassi, H. M. and Grzedzinski, J., "Unsteady Disturbances of Streaming Motions Around Bodies," *J. Fluid Mech.,* Vol. 209, Dec. 1989, pp. 385-403.
9. Jameson, A. and Caughey, D.A., "A Finite Volume Method for Transonic Potential Flow Calculations," *Proceedings of the AIAA 3rd Computational Fluid Dynamics Conference,* Williamsburg, Va., July 1979, pp. 122-146.
10. Atassi, H. M. and Scott, J. R., "Analysis of Nonuniform Subsonic Flows About a Row of Moving Blades," *Proceedings of the Fourth International Symposium on Unsteady Aerodynamics and Aeroelasticity of Turbomachines and Propellers,* H. E. Gallus and S. Servaty, eds., Institute fur Strahlantriebe und Turbomachine, University of Aachen, Federal Republic of Germany, 1988, pp. 39-67.
11. Scott, J. R. and Atassi, H. M., "Numerical Solution of Periodic Vortical Flows About a Thin Airfoil," AIAA Paper 89-1691, June, 1989.
12. Atassi, H.M., "Unsteady Vortical Disturbances Around Bodies," *Proceedings of the Tenth U. S. National Congress of Applied Mechanics,* J.P. Lamb, ed., ASME, 1986, pp. 475-484.
13. Atassi, H.M. and Grzedzinski, J., "Three-Dimensional Periodic Distortions of Flows Around Lifting Airfoils," University of Notre Dame Report, Aerodynamics Group, No. 8, 1986.
14. Sears, W. R., "Some Aspects of Non-stationary Airfoil Theory and Its Practical Applications." *J. Aero. Sci.,* Vol. 8, No. 3, 1941, pp. 104-108.
15. Scott, J.R., "Compressible Flows with Periodic Vortical Disturbances Around Lifting Airfoils," Ph. D. Dissertation, University of Notre Dame, Notre Dame, IN, 1990.

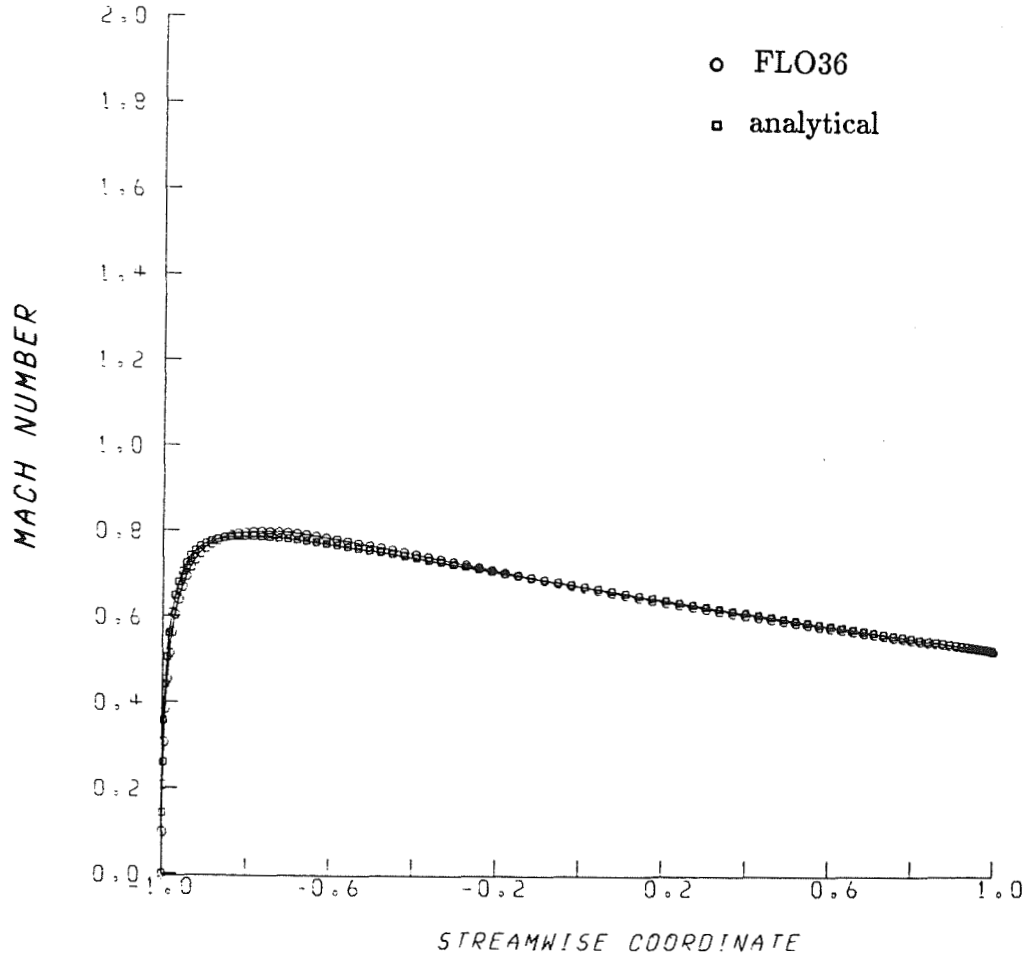

Figure 1. Comparison of Mach number at the airfoil surface between FLO36 and the present analytical scheme. $M_\infty = .6$, $\alpha = 0°$, camber = 0, thickness = .12.

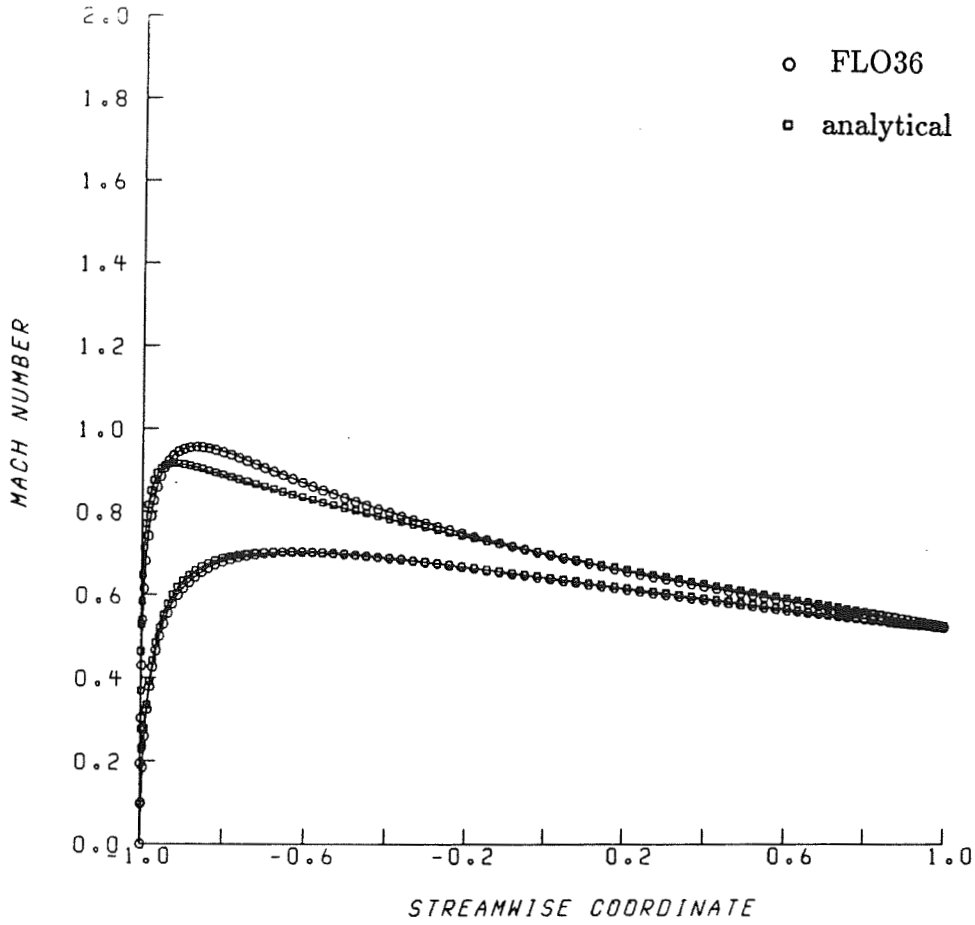

Figure 2. Comparison of Mach number at the airfoil surface between FLO36 and the present analytical scheme. $M_\infty = .6$, $\alpha = 2^o$, camber = 0, thickness = .12.

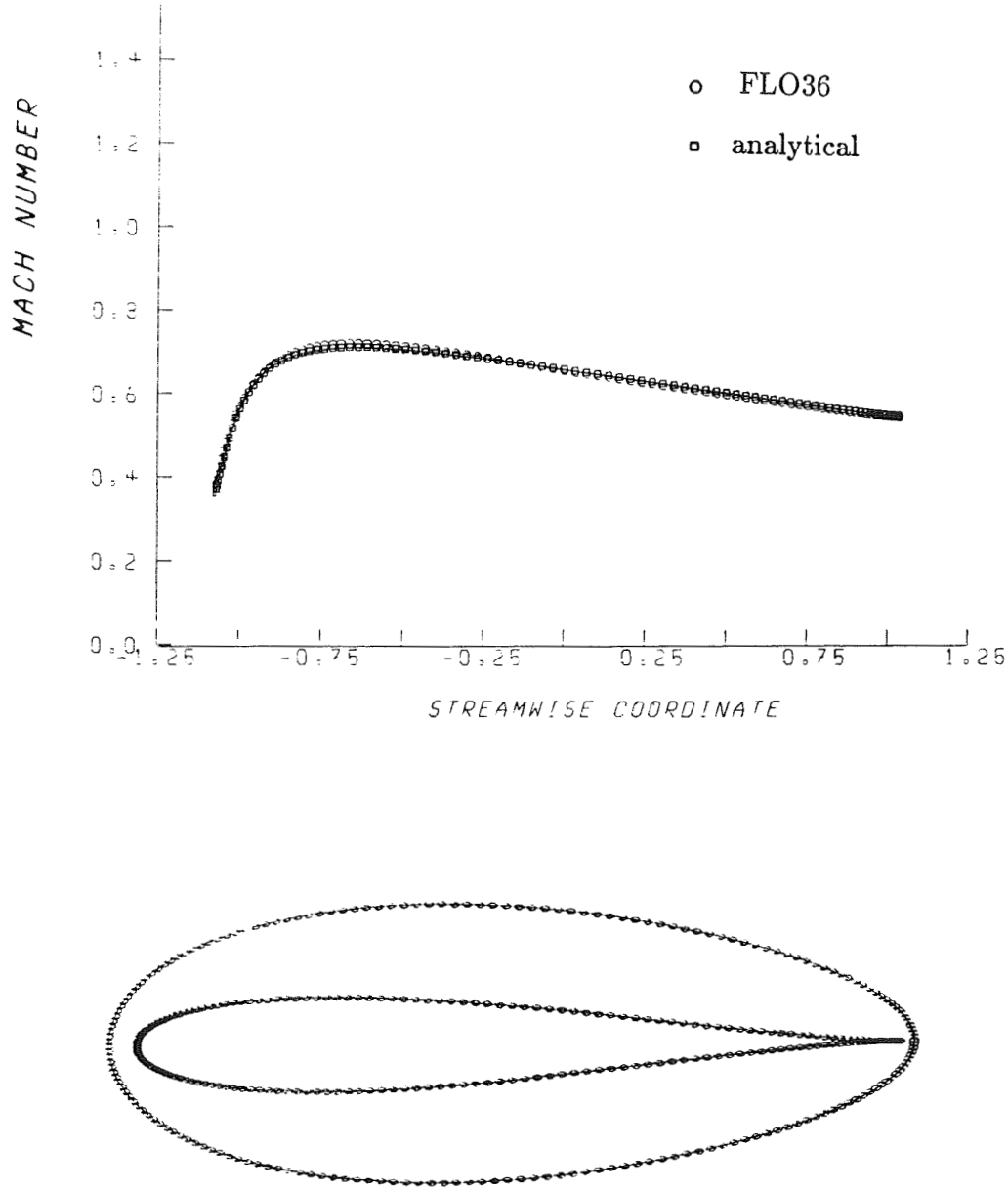

Figure 3. Comparison of Mach number along a FLO36 grid line which wraps around the airfoil. $M_\infty = .6$, $\alpha = 0°$, camber $= 0$, thickness $= .12$.

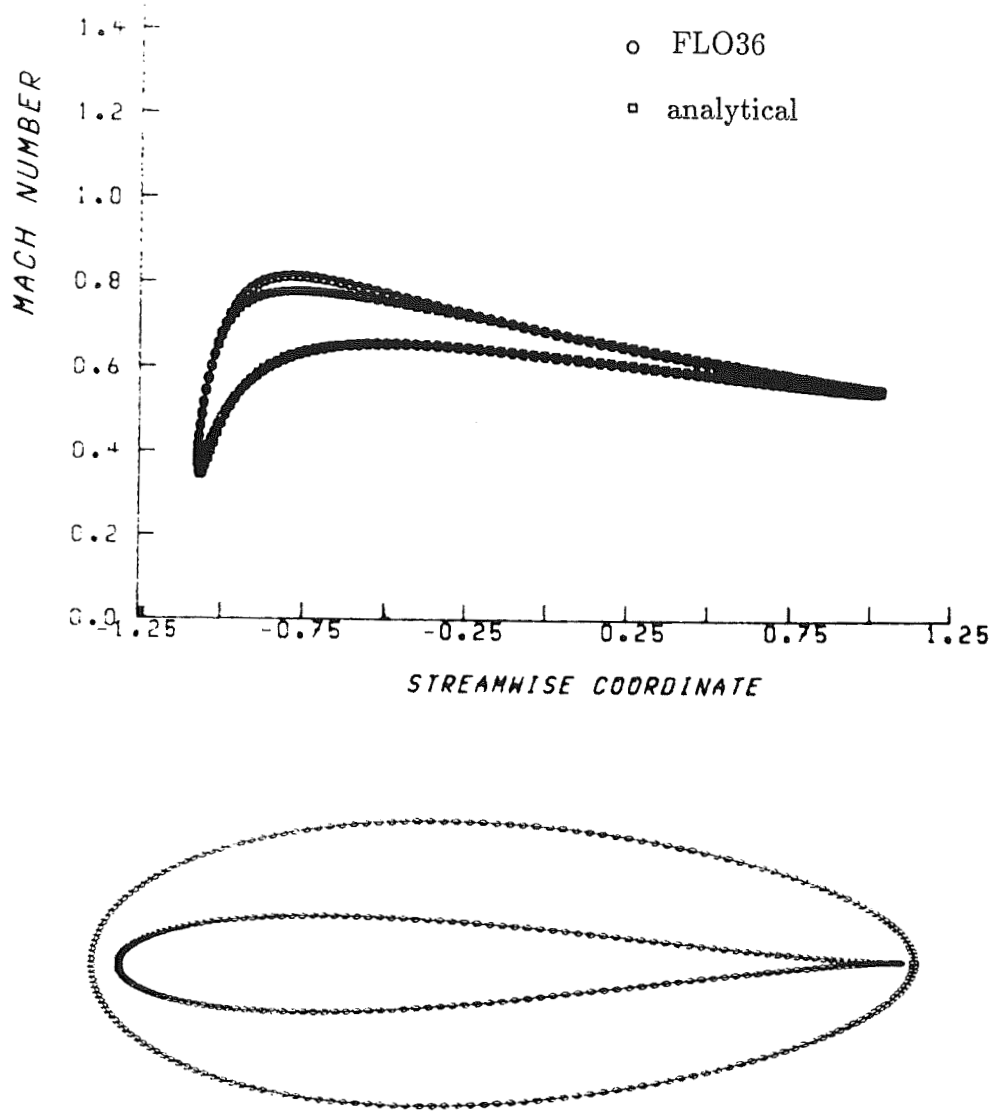

Figure 4. Comparison of Mach number along a FLO36 grid line which wraps around the airfoil. $M_\infty = .6$, $\alpha = 2^o$, camber = 0, thickness = .12.

C-2

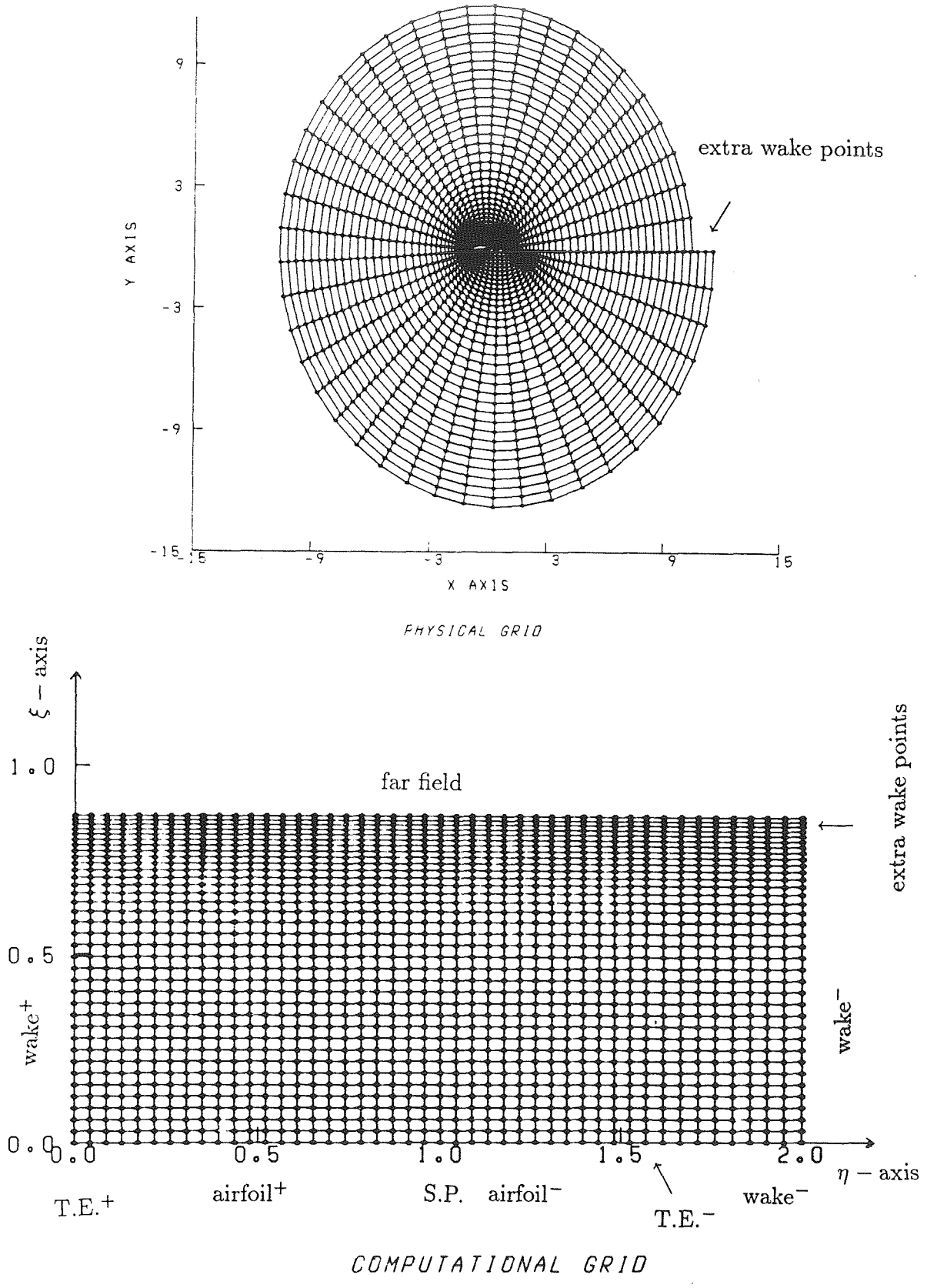

Figure 5. Computational and physical grids.

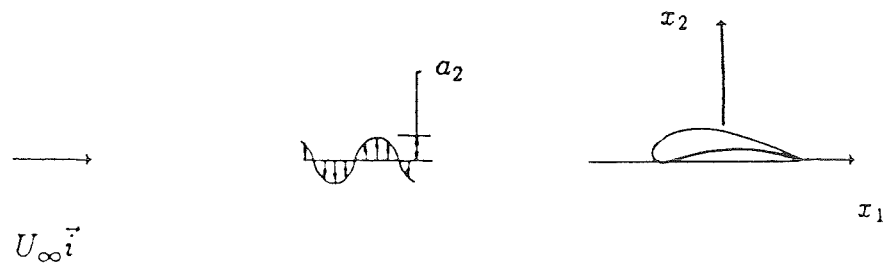

Figure 6. Airfoil in a transverse gust.

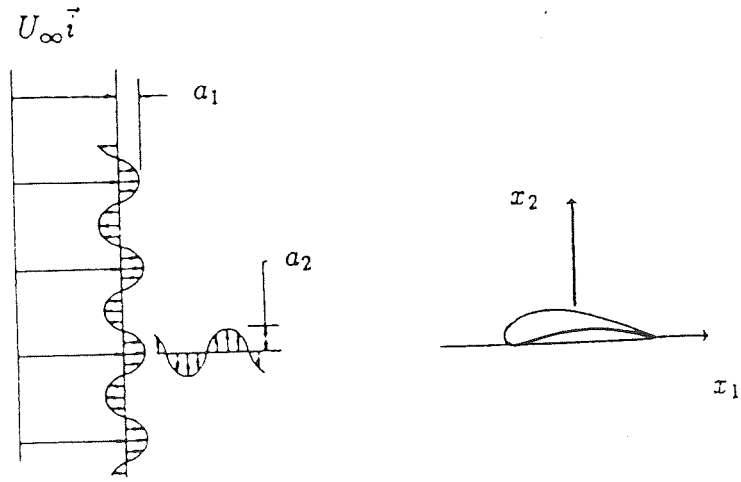

Figure 7. Airfoil in a transverse and longitudinal gust.

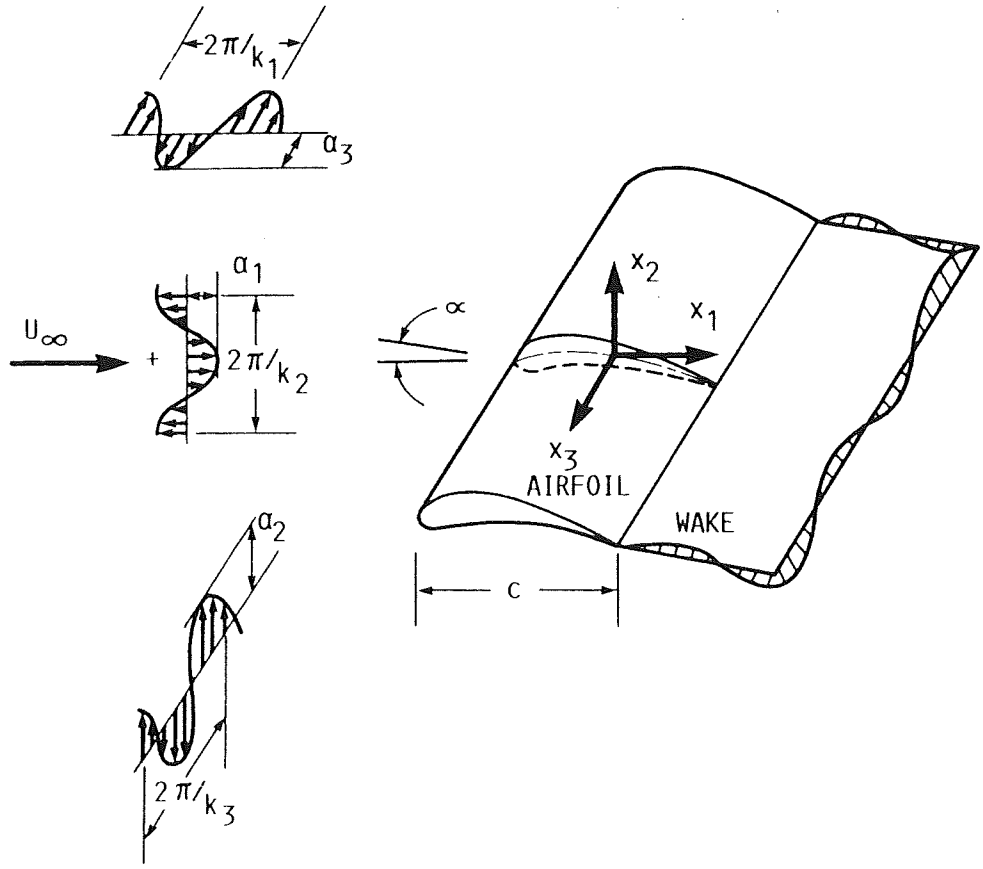

Figure 8. Airfoil in a three-dimensional gust.

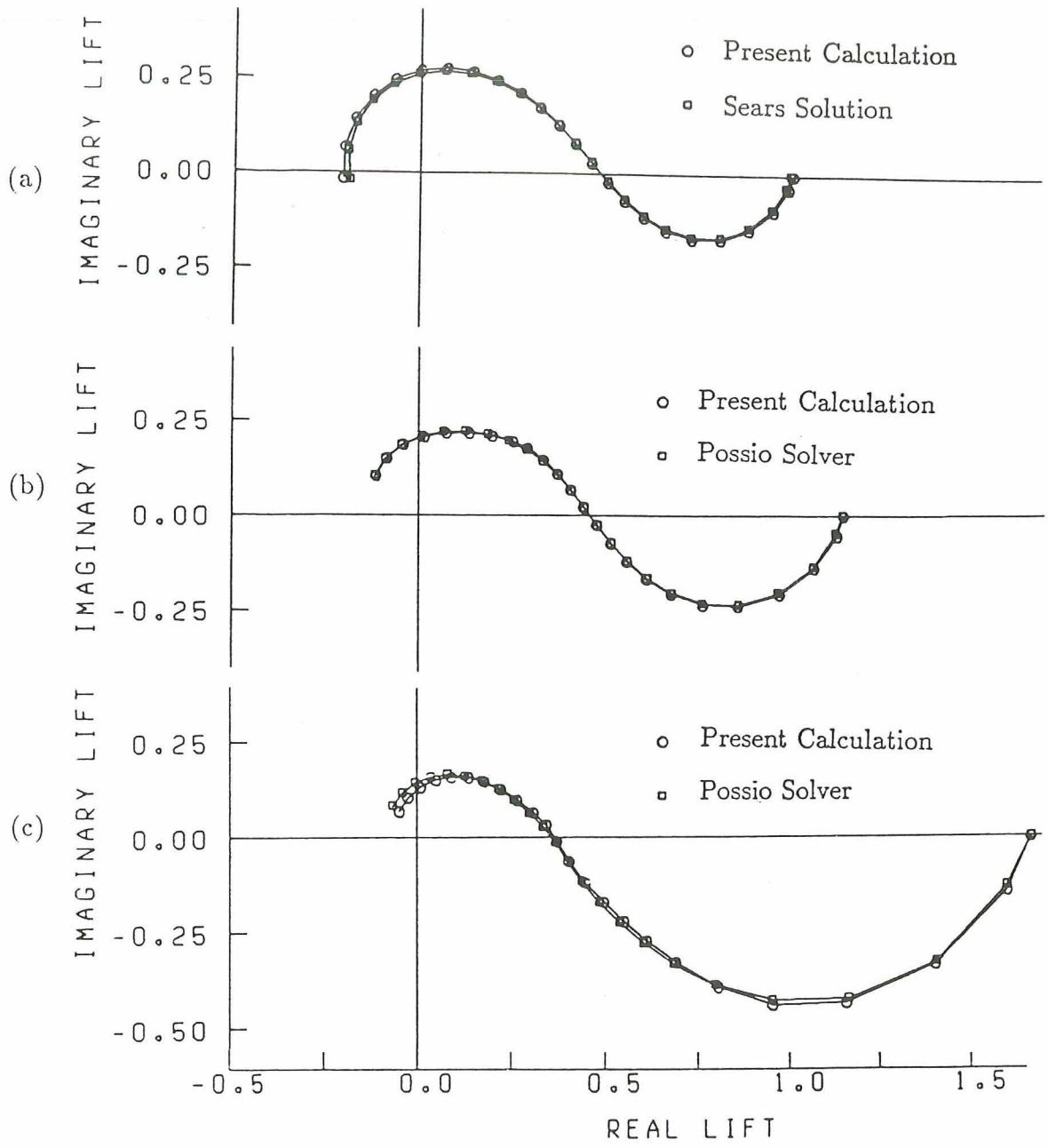

Figure 9. Comparison between the numerically computed unsteady lift and analytical results for a flat plate airfoil in a transverse gust at (a) $M = 0.1$, (b) $M = 0.5$, and (c) $M = 0.8$
$k_1 = 0.0, 0.007, 0.027, 0.062, 0.110, 0.172, 0.248, 0.338, 0.442, 0.561, 0.694, 0.842, 1.01, 1.18, 1.38, 1.59, 1.82, 2.07, 2.33, 2.62, 2.93, 3.26, 3.62, 4.01$

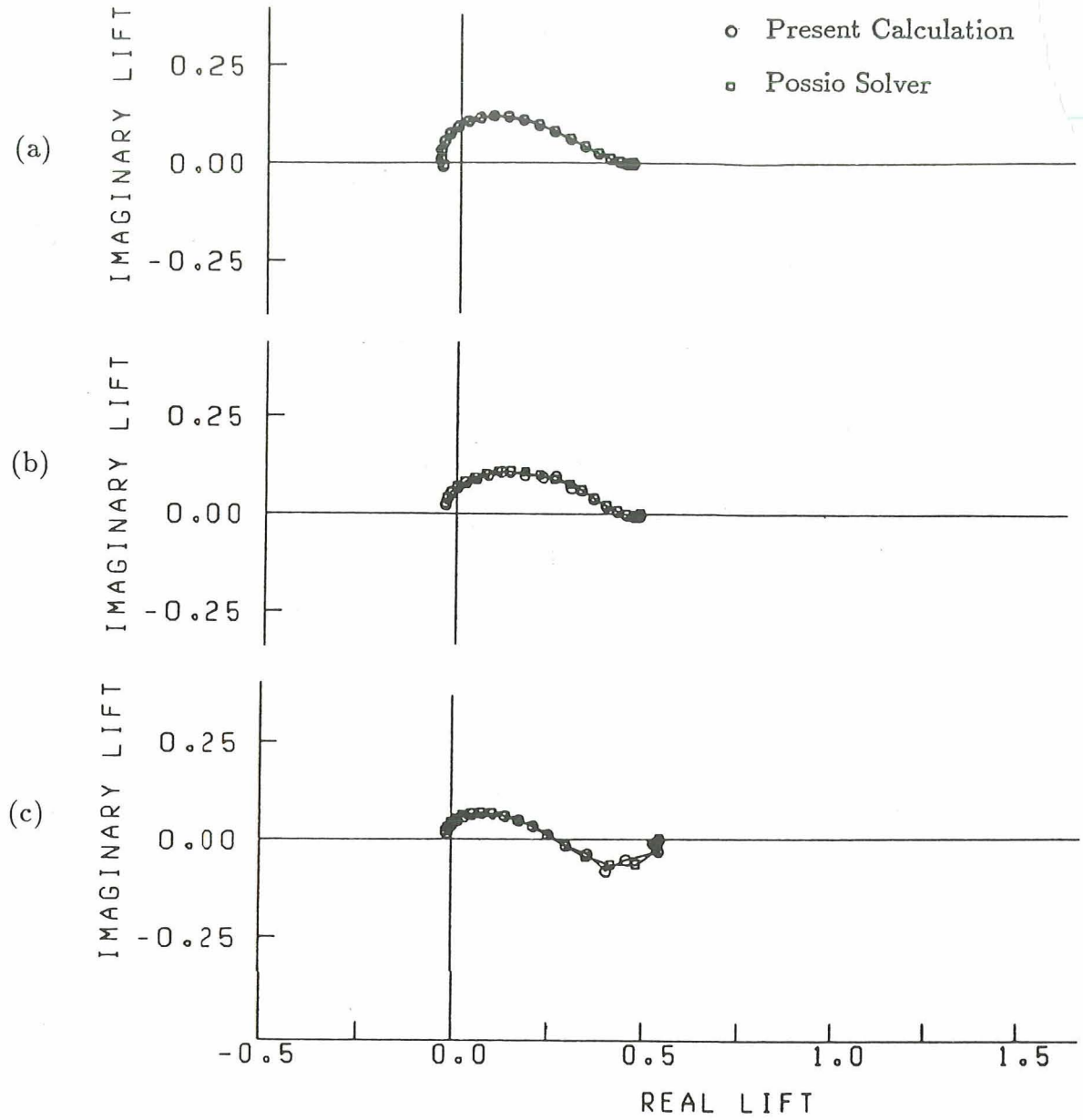

Figure 10. Comparison between the numerically computed unsteady lift and analytical results for a flat plate airfoil in a three-dimensional gust at (a) $M = 0.1$, (b) $M = 0.5$, and (c) $M = 0.8$
$k_3 = 0.442$, $|\vec{a}| = 1$, $\frac{a_2}{a_1} = -\frac{7}{4}$, $k_1 = k_2$, $\vec{a} \cdot \vec{k} = 0$, $a_2 > 0$
$k_1 = 0.0, 0.007, 0.027, 0.062, 0.110, 0.172, 0.248, 0.338, 0.442, 0.561, 0.694, 0.842, 1.01, 1.18, 1.38, 1.59, 1.82, 2.07, 2.33, 2.62, 2.93, 3.26, 3.62, 4.01$

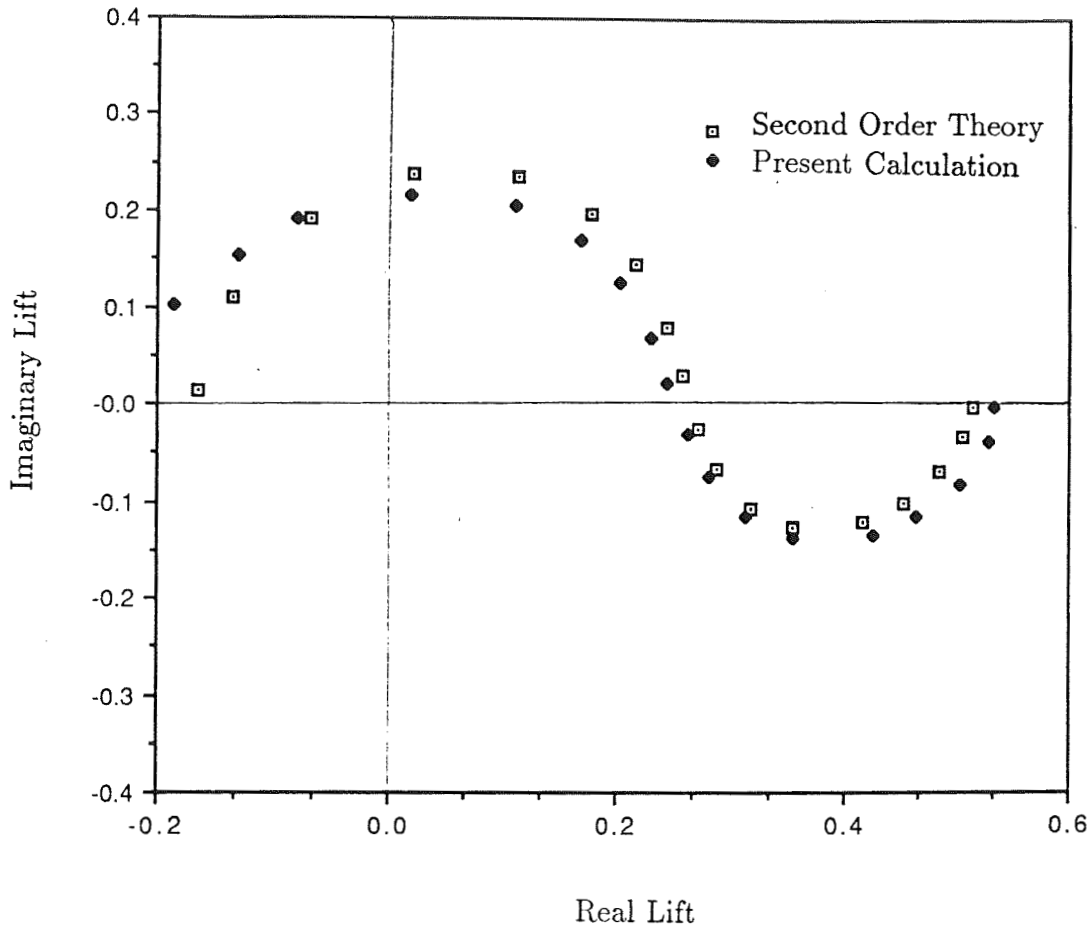

Figure 11. Comparison between the numerically computed unsteady lift and the second order theory for an airfoil in a transverse and longitudinal gust. The second order theory does not account for the thickness of the airfoil. $M_\infty = .1$, $\alpha = 2^o$, camber = .05, thickness ratio = .06. $-a_1 = a_2 = .7071$, $k_1 = k_2, a_3 = k_3 = 0$
k_1 = 0.0, 0.01, 0.03, 0.06, 0.1, 0.2, 0.3, 0.45, 0.6,
0.8, 1.0, 1.3, 1.6, 2.0, 2.5, 3.0, 3.5, 4.0

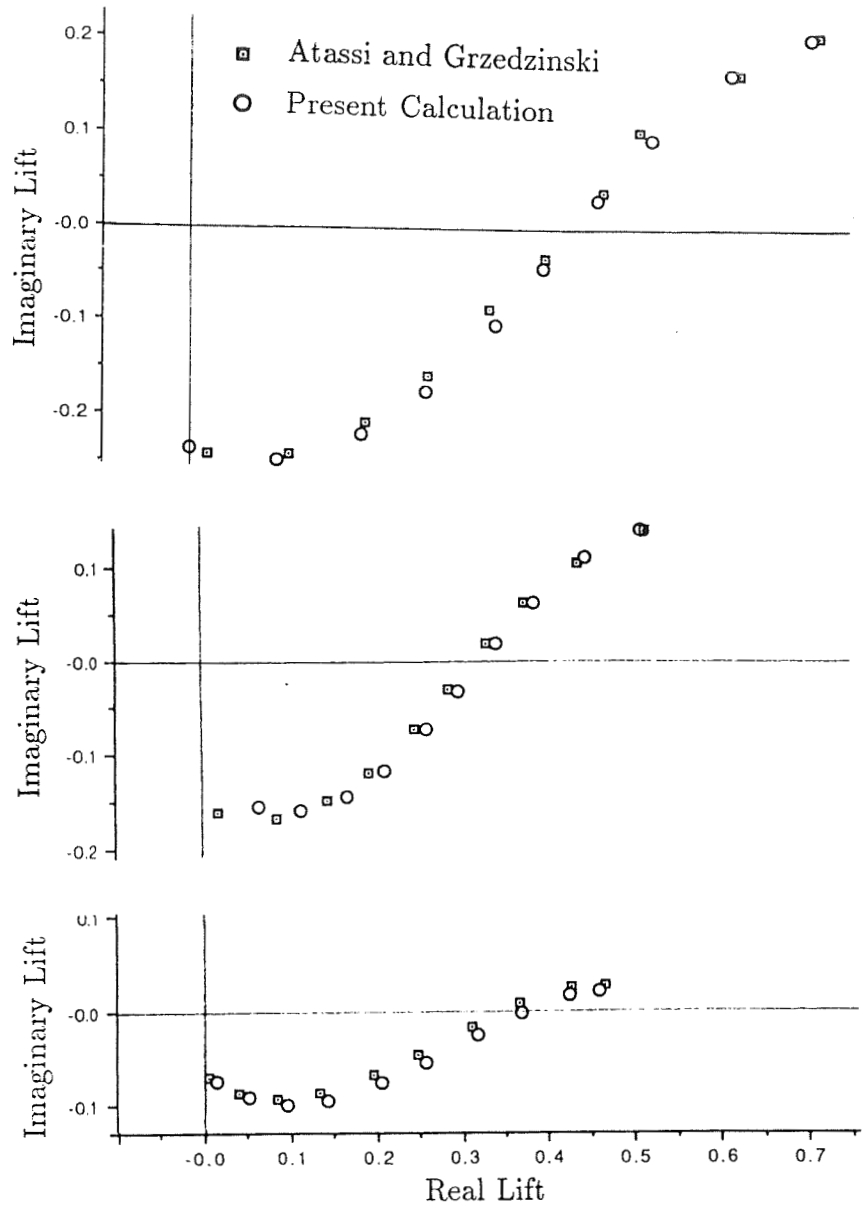

Figure 12. Comparison between the numerically computed unsteady lift and the first order results of Atassi and Grzedzinski for a (a) transverse gust, (b) transverse and longitudinal gust with $-a_1 = a_2 = .7071$, $k_1 = k_2$, $a_3 = k_3 = 0$, and (c) a three-dimensional gust with $k_3 = 0.4$, $|\vec{a}| = 1$, $\frac{a_2}{a_1} = -\frac{7}{4}$, $k_1 = k_2$, $\vec{a} \cdot \vec{k} = 0$, $a_2 > 0$. $M_\infty = .1$, $\alpha = 0$, camber = 0, thickness ratio = .12. Results shown are the complex conjugate values of the unsteady lift.

$k_1 = 0.2, 0.3, 0.45, 0.6, 0.8, 1.0, 1.3, 1.6, 2.0, 2.5$

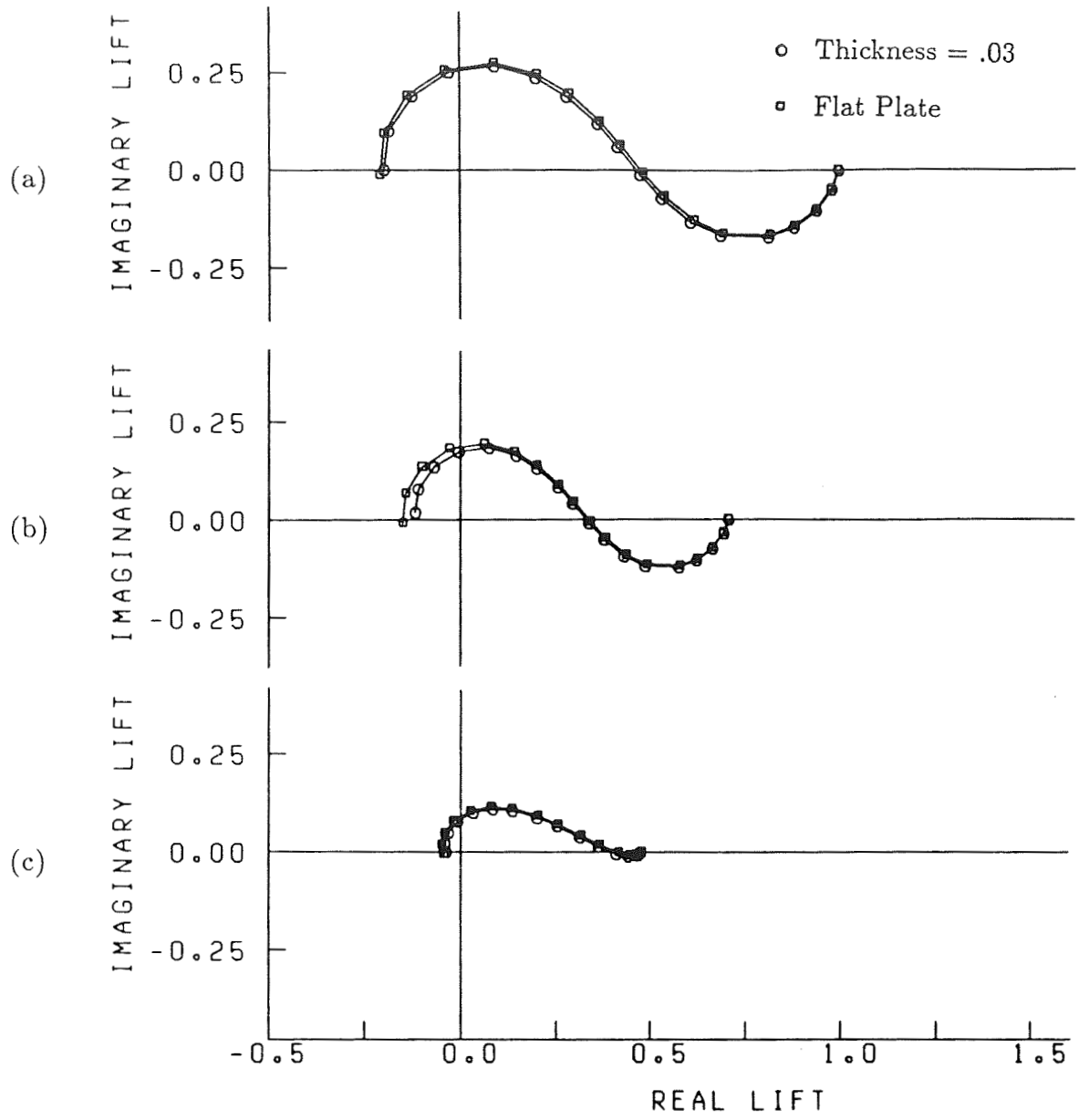

Figure 13. Comparison between the unsteady lift of a flat plate airfoil and a 3 percent thick Joukowski airfoil in a (a) transverse gust, (b) transverse and longitudinal gust with $-a_1 = a_2 = .7071$, $k_1 = k_2$, $a_3 = k_3 = 0$, and (c) a three-dimensional gust with $k_3 = 0.4$, $|\vec{a}| = 1$, $\frac{a_2}{a_1} = -\frac{7}{4}$, $k_1 = k_2$, $\vec{a} \cdot \vec{k} = 0$, $a_2 > 0$. $M_\infty = .1$, $\alpha = 0$, camber $= 0$. $k_1 = 0.0, 0.01, 0.03, 0.06, 0.1, 0.2, 0.3, 0.45, 0.6,$ $0.8, 1.0, 1.3, 1.6, 2.0, 2.5, 3.0, 3.5, 4.0$

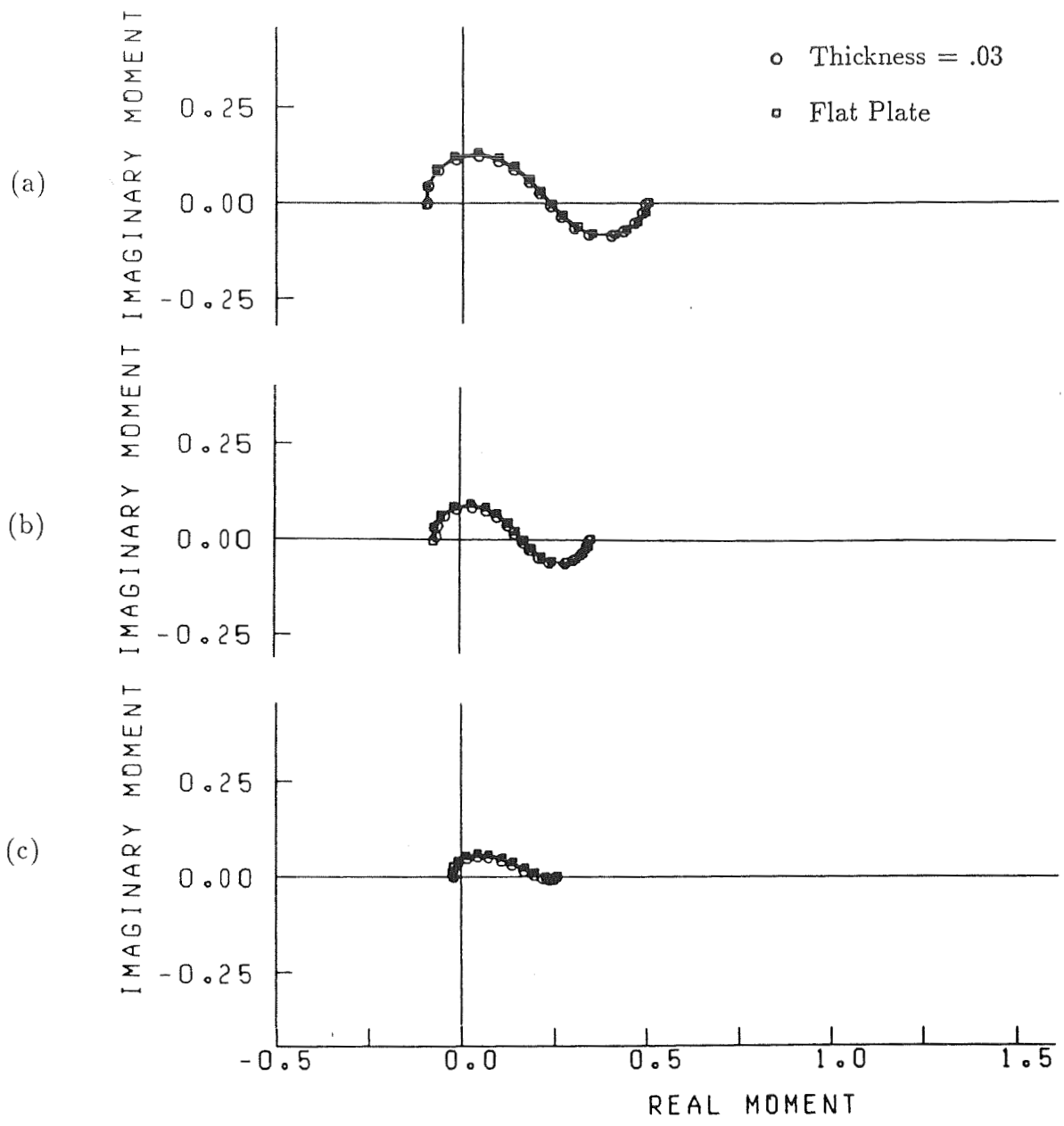

Figure 14. Comparison between the unsteady moment of a flat plate airfoil and a 3 percent thick Joukowski airfoil in a (a) transverse gust, (b) transverse and longitudinal gust with $-a_1 = a_2 = .7071$, $k_1 = k_2$, $a_3 = k_3 = 0$, and (c) a three-dimensional gust with $k_3 = 0.4$, $|\vec{a}| = 1$, $\frac{a_2}{a_1} = -\frac{7}{4}$, $k_1 = k_2$, $\vec{a} \cdot \vec{k} = 0$, $a_2 > 0$. $M_\infty = .1$, $\alpha = 0$, camber $= 0$. $k_1 =$ 0.0, 0.01, 0.03, 0.06, 0.1, 0.2, 0.3, 0.45, 0.6, 0.8, 1.0, 1.3, 1.6, 2.0, 2.5, 3.0, 3.5, 4.0

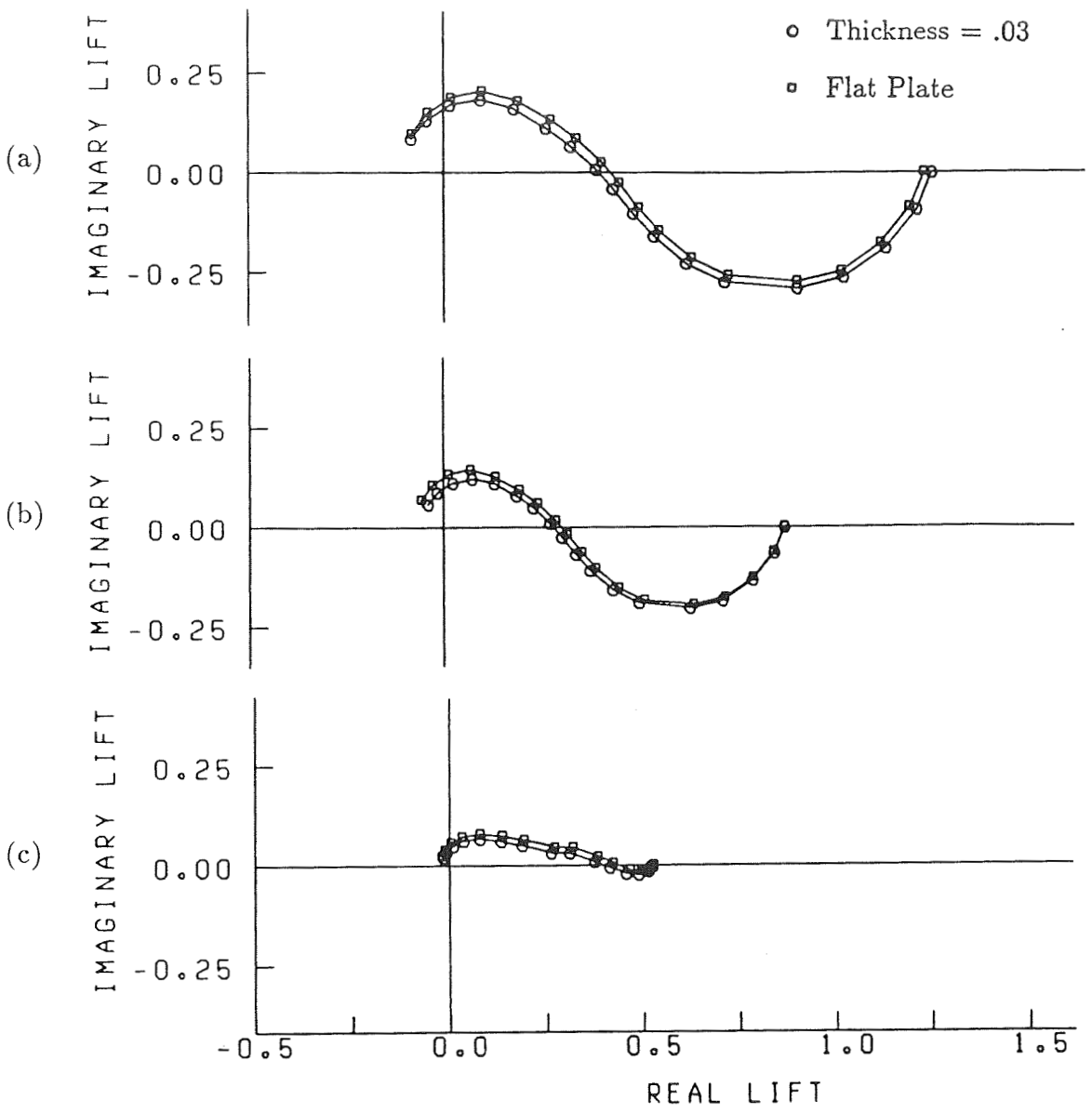

Figure 15. Comparison between the unsteady lift of a flat plate airfoil and a 3 percent thick Joukowski airfoil in a (a) transverse gust, (b) transverse and longitudinal gust with $-a_1 = a_2 = .7071$, $k_1 = k_2$, $a_3 = k_3 = 0$, and (c) a three-dimensional gust with $k_3 = 0.4$, $|\vec{a}| = 1$, $\frac{a_2}{a_1} = -\frac{7}{4}$, $k_1 = k_2$, $\vec{a} \cdot \vec{k} = 0$, $a_2 > 0$. $M_\infty = .6$, $\alpha = 0$, camber $= 0$. $k_1 = 0.0, 0.01, 0.03, 0.06, 0.1, 0.2, 0.3, 0.45, 0.6,$ $0.8, 1.0, 1.3, 1.6, 2.0, 2.5, 3.0, 3.5, 4.0$

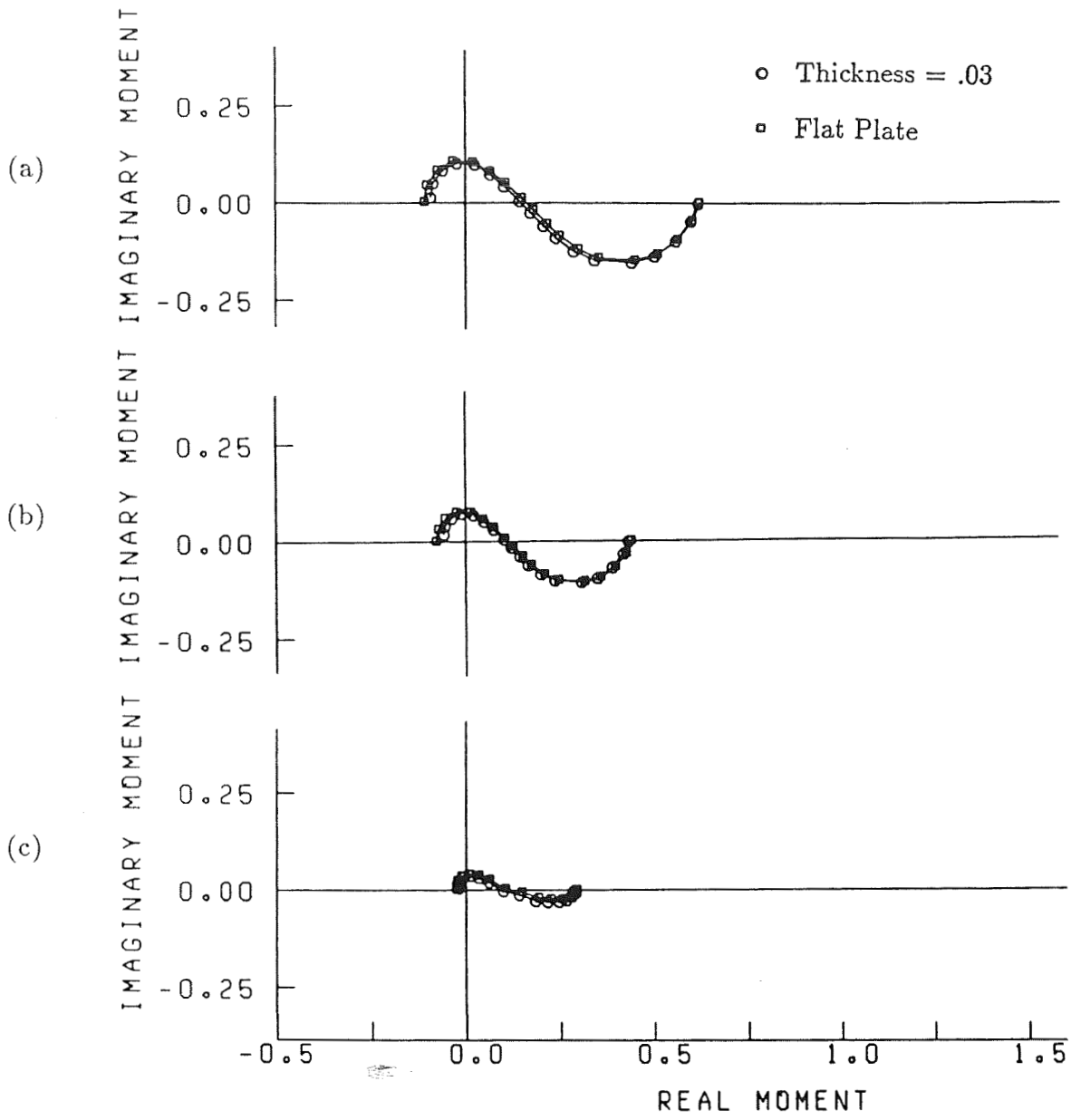

Figure 16. Comparison between the unsteady moment of a flat plate airfoil and a 3 percent thick Joukowski airfoil in a (a) transverse gust, (b) transverse and longitudinal gust with $-a_1 = a_2 = .7071$, $k_1 = k_2$, $a_3 = k_3 = 0$, and (c) a three-dimensional gust with $k_3 = 0.4$, $|\vec{a}| = 1$, $\frac{a_2}{a_1} = -\frac{7}{4}$, $k_1 = k_2$, $\vec{a} \cdot \vec{k} = 0$, $a_2 > 0$. $M_\infty = .6$, $\alpha = 0$, camber $= 0$. $k_1 = 0.0, 0.01, 0.03, 0.06, 0.1, 0.2, 0.3, 0.45, 0.6,$ $0.8, 1.0, 1.3, 1.6, 2.0, 2.5, 3.0, 3.5, 4.0$

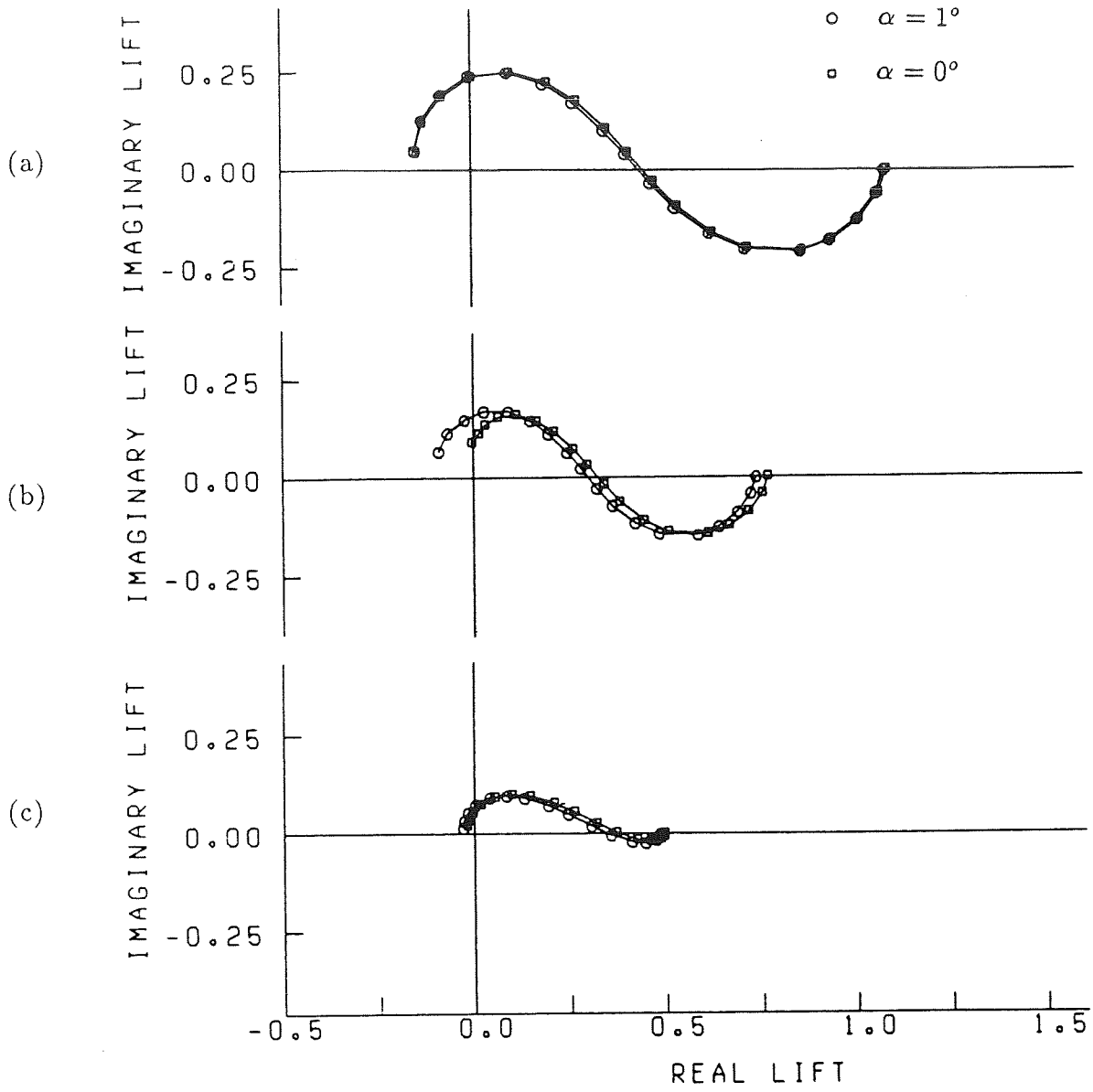

Figure 17. Comparison between the unsteady lift of a 12 percent thick, Joukowski airfoil at 0^o angle of attack and 1^o angle of attack for a (a) transverse gust, (b) transverse and longitudinal gust with $-a_1 = a_2 = .7071$, $k_1 = k_2$, $a_3 = k_3 = 0$, and (c) a three-dimensional gust with $k_3 = 0.4$, $|\vec{a}| = 1$, $\frac{a_2}{a_1} = -\frac{7}{4}$, $k_1 = k_2$, $\vec{a} \cdot \vec{k} = 0$, $a_2 > 0$. $M_\infty = .1$, camber = 0, thickness ratio = .12.

k_1 = 0.0, 0.01, 0.03, 0.06, 0.1, 0.2, 0.3, 0.45, 0.6,
0.8, 1.0, 1.3, 1.6, 2.0, 2.5, 3.0, 3.5, 4.0

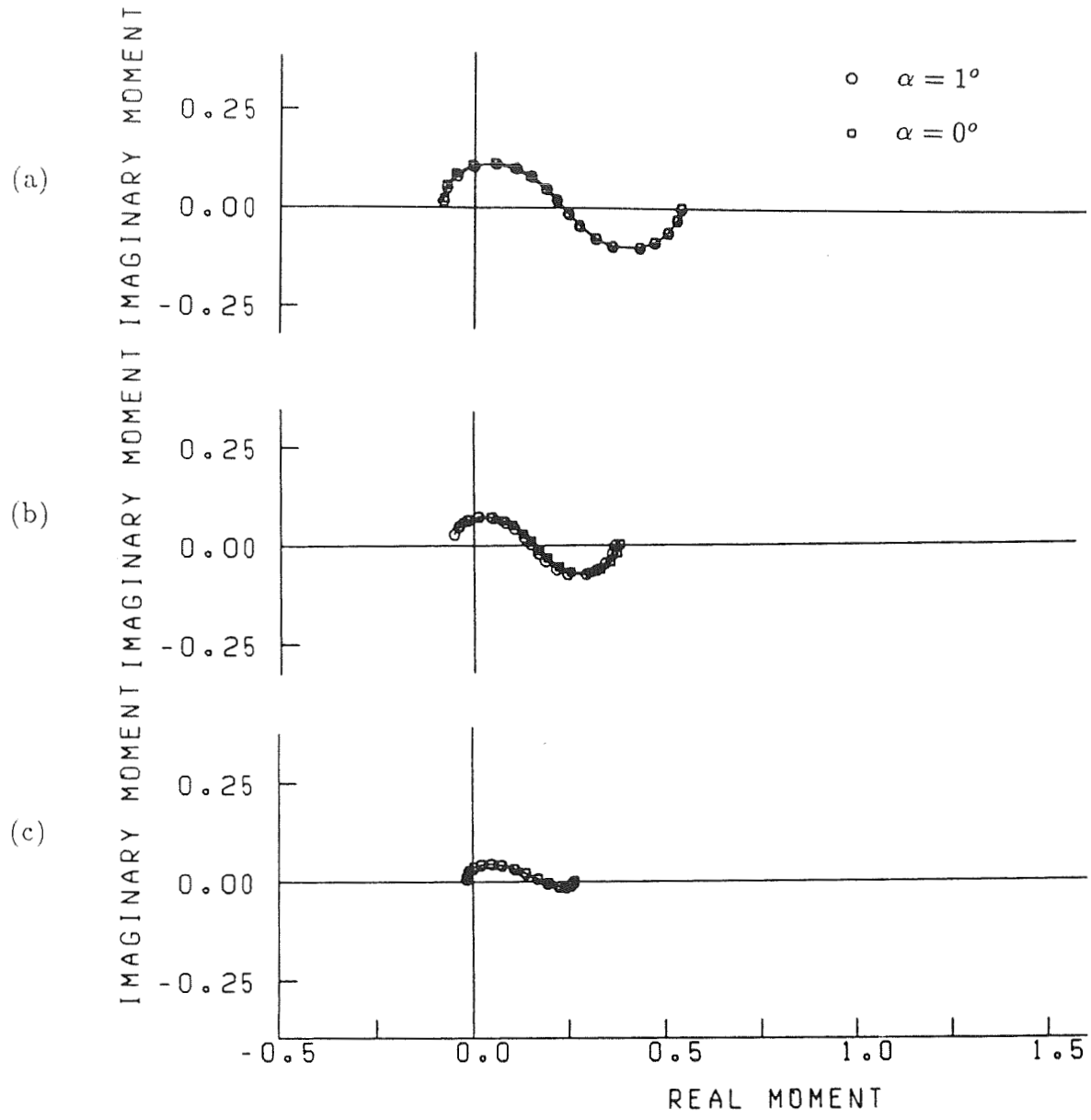

Figure 18. Comparison between the unsteady moment of a 12 percent thick, Joukowski airfoil at 0^o angle of attack and 1^o angle of attack for a (a) transverse gust, (b) transverse and longitudinal gust with $-a_1 = a_2 = .7071$, $k_1 = k_2$, $a_3 = k_3 = 0$, and (c) a three-dimensional gust with $k_3 = 0.4$, $|\vec{a}| = 1$, $\frac{a_2}{a_1} = -\frac{\tau}{4}$, $k_1 = k_2$, $\vec{a} \cdot \vec{k} = 0$, $a_2 > 0$. $M_\infty = .1$, camber = 0, thickness ratio = .12.

k_1 = 0.0, 0.01, 0.03, 0.06, 0.1, 0.2, 0.3, 0.45, 0.6, 0.8, 1.0, 1.3, 1.6, 2.0, 2.5, 3.0, 3.5, 4.0

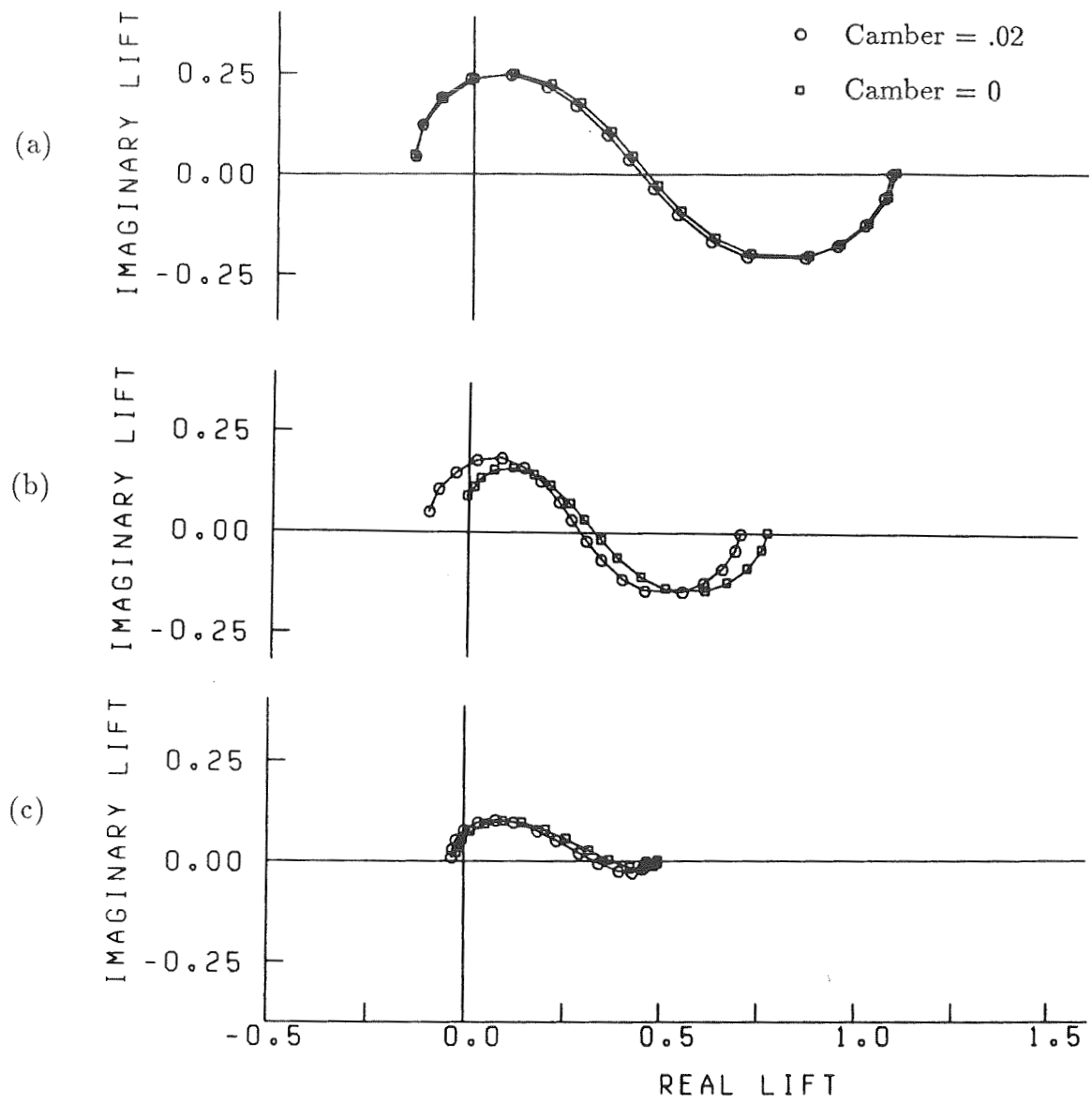

Figure 19. Comparison between the unsteady lift of an uncambered Joukowski airfoil and an airfoil with camber ratio of .02 for a (a) transverse gust, (b) transverse and longitudinal gust with $-a_1 = a_2 = .7071$, $k_1 = k_2$, $a_3 = k_3 = 0$, and (c) a three-dimensional gust with $k_3 = 0.4$, $|\vec{a}| = 1$, $\frac{a_2}{a_1} = -\frac{7}{4}$, $k_1 = k_2$, $\vec{a} \cdot \vec{k} = 0$, $a_2 > 0$. $M_\infty = .1$, $\alpha = 0^o$, thickness ratio = .12.

k_1 = 0.0, 0.01, 0.03, 0.06, 0.1, 0.2, 0.3, 0.45, 0.6,
0.8, 1.0, 1.3, 1.6, 2.0, 2.5, 3.0, 3.5, 4.0

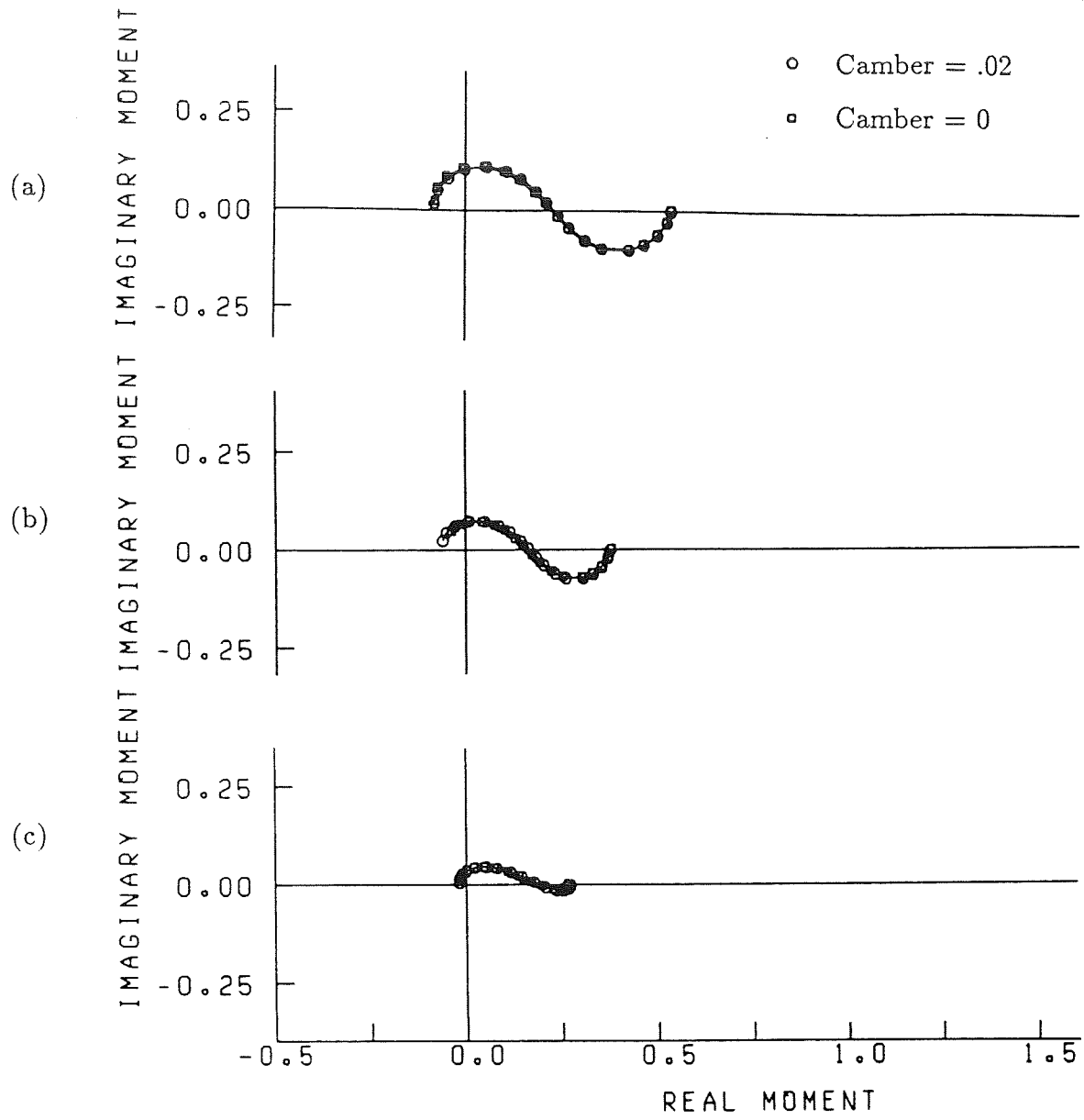

Figure 20. Comparison between the unsteady moment of an uncambered Joukowski airfoil and an airfoil with camber ratio of .02 for a (a) transverse gust, (b) transverse and longitudinal gust with $-a_1 = a_2 = .7071$, $k_1 = k_2$, $a_3 = k_3 = 0$, and (c) a three-dimensional gust with $k_3 = 0.4$, $|\vec{a}| = 1$, $\frac{a_2}{a_1} = -\frac{7}{4}$, $k_1 = k_2$, $\vec{a} \cdot \vec{k} = 0$, $a_2 > 0$. $M_\infty = .1$, $\alpha = 0^o$, thickness ratio = .12.

k_1 = 0.0, 0.01, 0.03, 0.06, 0.1, 0.2, 0.3, 0.45, 0.6,
0.8, 1.0, 1.3, 1.6, 2.0, 2.5, 3.0, 3.5, 4.0

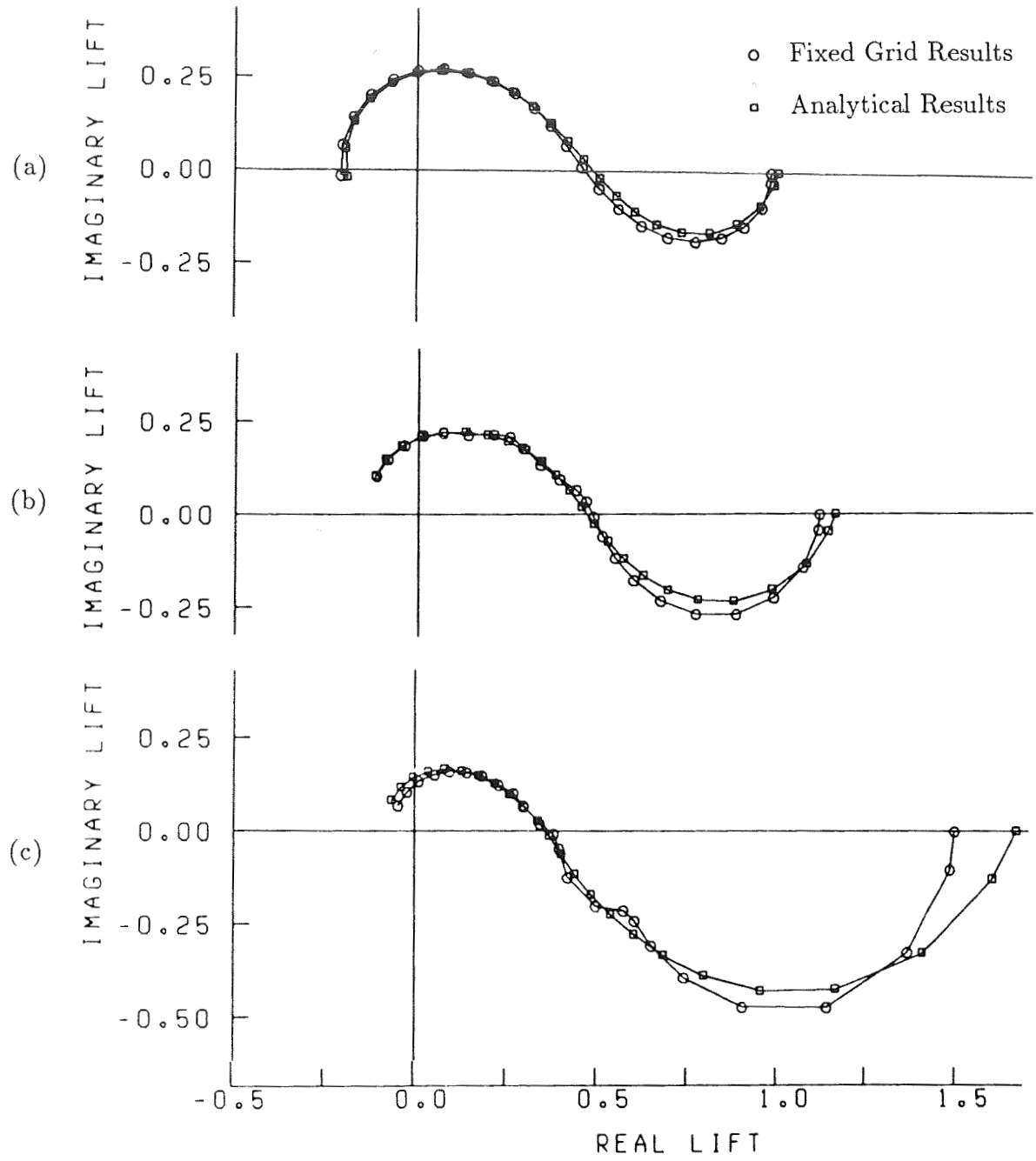

Figure 21. Comparison between numerical results generated on a fixed grid and analytical results for a flat plate airfoil in a transverse gust at (a) $M = 0.1$, (b) $M = 0.5$, and (c) $M = 0.8$.

$k_1 = 0.0, 0.007, 0.027, 0.062, 0.110, 0.172, 0.248, 0.338, 0.442, 0.561, 0.694, 0.842, 1.01, 1.18, 1.38, 1.59, 1.82, 2.07, 2.33, 2.62, 2.93, 3.26, 3.62, 4.01$

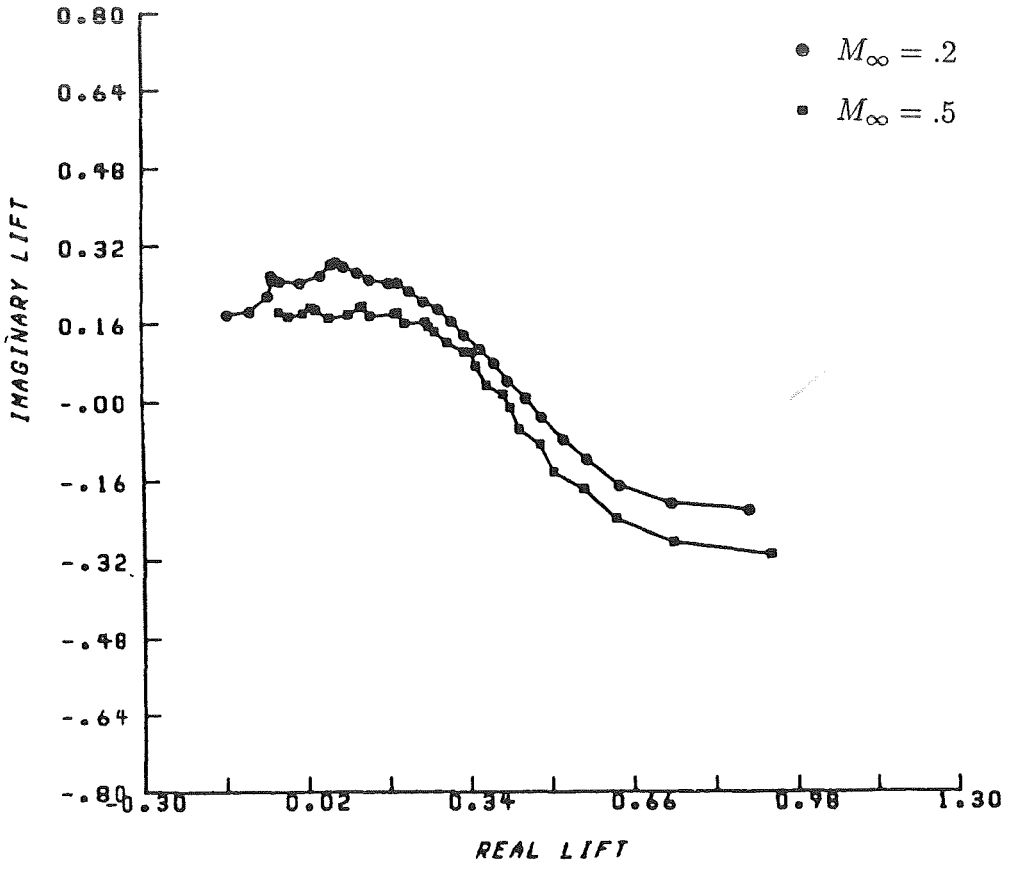

Figure 22. Numerical results for the unsteady lift of a 12 percent thick, symmetric Joukowski airfoil in a transverse gust. Results show grid dependent errors due to exponentially decreasing spacing in the ξ direction which was used in place of condition (3.70).

$k_1 = 0.1, 0.2, 0.3, 0.4, 0.5, 0.6, 0.7, 0.8, 0.9, 1.0,$
$1.1, 1.2, 1.3, 1.4, 1.5, 1.6, 1.7, 1.8, 1.9, 2.0,$
$2.1, 2.2, 2.3, 2.4, 2.5, 2.6, 2.7, 2.8, 2.9, 3.0$